Lehigh University
Lehigh Preserve

Theses and Dissertations

2008

Graphite like C5N : synthesis, characterization, intercalation, and comparison with graphite analogs

Wade H. Bailey
Lehigh University

Follow this and additional works at: http://preserve.lehigh.edu/etd

Recommended Citation
Bailey, Wade H., "Graphite like C5N : synthesis, characterization, intercalation, and comparison with graphite analogs" (2008). *Theses and Dissertations.* Paper 1024.

This Thesis is brought to you for free and open access by Lehigh Preserve. It has been accepted for inclusion in Theses and Dissertations by an authorized administrator of Lehigh Preserve. For more information, please contact preserve@lehigh.edu.

Bailey, Wade H., III

Graphite-Like C_5N: Synthesis, Characterization, Intercalation, and Comparison with Graphite Analogs

January 2009

Graphite-Like C_5N: Synthesis, Characterization, Intercalation, and Comparison with Graphite Analogs

By

Wade H. Bailey III

A Thesis

Presented to the Graduate and Research Committee

of Lehigh University

in Candidacy for the Degree of

Master of the Sciences

in

Chemistry

Lehigh University

November 2008

Under The Direction of

Dr. Kai Landskron, Lehigh University

and

Dr. Guido Pez, Air Products and Chemicals, Inc.

Thesis Signature Sheet

Approved and recommended for acceptance as a thesis in partial fulfillment of the requirements for the Degree of Master of the Sciences in Chemistry.

12/3/08

Date

Thesis Advisor: Dr. Kai Landskron

Co-Advisor: Dr. Rebecca Miller

Department Chairperson: Dr. Robert Flowers

Acknowledgements

The endeavor of learning cannot be successful without those who care to share their expertise, time, support, and tolerance for those who seek knowledge. I am thankful for the opportunity to matriculate under Dr. Kai Landskron with the help and support of my fellow students Le Li, Lili Liu, and Dr. Paritosh Mohanty. My appreciation is also extended to the Administration and supporting Deans of Lehigh University. Also, this work would not have been possible without the support, materials, and facilities at Air Products. The leadership and wisdom of Guido Pez, Bill Casteel, Alan Cooper, and Garret Lau have been invaluable in the support of this project. Many of the analytical techniques utilized in this investigation were new to me and would not have been possible without the teachings of a number of analytical experts including Peter DeSanto (STEM/EELS), Lin-Shu Du (Solid-state NMR), Robert Haney (XPS), Gary Johnson (Vibrational spectroscopy), Jim Stets (Electron Microscopy), and David Doetschman (Electron paramagnetic resonance, SUNY, Binghamton, NY). I am grateful for the guidance of Steven Mayorga and Bill Casteel for their insights into Dr. Bartlett's group during the time that graphite-like C_5N was originally devised and discovered; the hard work and careful documentation of Dr. Ciping Shen is noted as a necessary reference for reproducing the syntheses described. This investigation would not have been possible were it not for the powerful legacy left by the late Dr. Neil Bartlett. I cannot finish this written thesis without acknowledging my wife, Julie, for her unending support, patience, and love enabling me to complete my degree.

Table of Contents

List of Tables and Figures

Abstract

In following the use of graphite through history as it evolved from a simple writing implement to being used in advanced electronics and secondary storage batteries, graphitic materials continue to be developed and modified. For the current study electron rich graphite-like carbon nitride, C_5N, is synthesized and evaluated for the associated properties. Repeating the literature-prescribed synthesis of C_5N (Pyrolytic condensation of pyridine with chlorine) required method optimization which gave rise to the discovery of a key kinetic factor in producing large quantities of the pyrolytic carbon in high purities by affecting high utilization of the chlorine gas. Extensive analysis of this C_5N confirms its highly amorphous structure to be composed of sp^2 carbon containing an equal distribution of sp^3 and sp^2 nitrogen centers. Determining the nature of the amorphous C_5N required direct contrast with graphite but was not directly possible without also comparing to a pyrolytic carbon produced similarly to C_5N (reaction of benzene with chlorine). Each of the three carbons was reacted with the powerful intercalant, $S_2O_6F_2$, in order to evaluate the extent of graphitic character and the fate of the nitrogen. The presence of graphitic domains was confirmed to be minimal and contrary to expectations, oxidation with $S_2O_6F_2$ did not react at the nitrogen atom to affect rehybridization but rather bonded to carbon, indicating a much more settled electronic structure than originally believed. In order to unlock the full potential of such a material and understand it from a true fundamental level, it will be necessary in future work to provide C_5N in a highly ordered format in order to validate its structure.

Introduction

Graphite, one of the basic forms of carbon, has been a material of interest and importance for a considerable amount of time having appeared in an array of commercial products ranging from pencils to lithium storage batteries. Today, many forms of natural and synthetic graphites are known and have been exhaustively studied and characterized. The substitution of graphite with more electropositive elements, such as the extensively studied systems containing boron, disrupts the aromaticity of the graphene sheets in the neutral state but is practically restored when the boron or similar atom adopts a negative charge. Constituting an area of considerably less research are the more electron-rich graphite materials, especially those substituted or doped with nitrogen. These are conversely affected and may very well be homologous and isoelectronic with graphite when the nitrogen, or similar atom, bears a positive charge and an appropriate counter ion is present. As will be seen in the following supporting information, existing reports of graphitic nitrogen-containing carbons are limited to those having extremely limited nitrogen content except for the graphite-like C_5N reported in the 1980's; this includes enough nitrogen to perceptibly influence its bulk chemical properties. Thus, this work covers carbon-nitrogen, C_5N, graphite research of which the target is to develop fundamental knowledge and experience regarding its chemical and structural nature. This study was made possible by the application of improved analytical techniques and attempts of comparative intercalation with peroxydisulfuryl difluoride.

Background

Graphite-like C_5N was first reported in 1986 by Bartlett and colleagues[1] giving little description of experimental methodologies. A following publication from the same group[2]

provided few additional details. Their final publication, in the form of a dissertation[3], contained considerable detail that was missing in the former communications. In general, the C_5N material was synthesized by the reaction of pyridine [Equation 1] with chlorine at temperatures greater than 680°C in an atmospheric-pressure, chemical vapor deposition (CVD), flow reactor.

$$C_5H_5N + 5/2\ Cl_2 \rightarrow C_5N + 5\ HCl \qquad \textbf{Equation 1}$$

The high temperatures for this conversion are necessary as the reaction of chlorine with pyridine at sub-ambient temperatures produces the pyridine-chlorine complex that decomposes [Equation 2] to the chlorinated pyridine upon warming[4]. These are the same products that are afforded by room temperature[5] combination of pyridine and chlorine.

$$C_5H_5N + Cl_2 \rightarrow [C_5H_5N : Cl_2] \rightarrow C_5H_4ClN + HCl \qquad \textbf{Equation 2}$$

Ideally, an ordered graphite with planar pyridine rings would be obtained based on the concept that benzene should react with chlorine to provide graphite and volatile HCl with quite a favorable free energy [Equation 3].

$$C_6H_6 + 3\ Cl_2 \rightarrow \text{Graphite} + 6\ HCl\ \ \Delta G^\circ = -27.92\ \text{kcal/mol} \qquad \textbf{Equation 3}$$

Attempts of this latter reaction were not reported by this group nor were any comparisons of the C_5N produced experimentally with graphite synthesized as such.

In these original studies, C_5N was characterized by powder X-ray diffraction (XRD), electrical resistance/conductivity, X-ray photoelectron spectroscopy (XPS), density, Auger electron spectroscopy (AES), and electron energy loss spectroscopy (EELS). While intercalation of other graphitic materials was routinely attempted[6] with the powerfully oxidizing $S_2O_6F_2$ to demonstrate graphene stacking, there is only one publication which broadly alludes that this was also attempted with C_5N[7] but no data was provided. In this context of potential C_5N intercalates it was only directly stated that the C_5N material did not uptake elemental bromine

as some other graphitic materials had. All of this analytical work led to the conclusion that that a poorly crystalline (i.e. amorphous), non-uniform, non-ordered, non-volatile, π-conjugated, conducting material with C_5N stoichiometry was formed. The graphite-like character was attributed to experimental comparison with graphitic B/C/N compositions and the formation of highly ordered graphite with thermal treatment and decomposition of C_5N at extreme temperatures which unfortunately also forced out the contained nitrogen.

Using similar chemistry and techniques during the same time period, Labes and colleagues reported graphite-like CVD products from the high temperature reaction of various aromatic hydrocarbons and heterocycles with halogens or thermolysis of halogenated aromatics[8,9,10,11,12,13]. Aside from also producing and example of reacting pyridine with chlorine as mentioned above, this group extended the comparison to other aromatics, including benzene, and demonstrated the viability of using elemental bromine as an alternate halogen source. In addition to some of the characterization techniques used by Bartlett's group, Labes and coworkers employed Raman spectroscopy and electron spin resonance (ESR or EPR for electron paramagnetic resonance) spectroscopy. The conclusions regarding the nature of the CVD-synthesized materials were similar to those proposed by Bartlett's group. It is noteworthy to point out that Labes' group had previously worked on the synthesis and pyrolysis of poly-cyanogen to afford a material of approximate composition C_5N[14,15,16,17]. Reporting relatively high yields, the products of pyrolysis were analyzed by UV-Vis, IR spectroscopy, and electrical conductivity providing sufficient evidence for the authors to claim a certain degree of graphitic character for the materials. Despite the relatively limited analytical support for Labes' C_5N materials, it is possible that these might be structurally similar to those formed by the halogen

condensation reactions. Nonetheless, no attempts to intercalate any of the materials made by Labes, et al. have been reported.

Chemical Abstract Services (CAS) was used to determine other sources that cited the key references noted above. A majority of the returned citations represented papers that were focused on the B/C/N systems[18,19,20] that Bartlett and coworkers included in their original publications. Most of the references that focused on CN systems were found to be concerned with the theoretical[21], diamond-like carbon nitride, C_3N_4, networked solids[22,23,24,25,26] noting that C_5N and its analogs are too devoid of nitrogen to be of any interest for this particular endeavor. Some search results included those covering CN materials with a nitrogen content considerably lower than C_5N[27]; those where CN films were coated over graphite[28], one in particular where a comparative and idealized C_5N bonding structure is proposed[29]. Some where CN materials were studied electrochemically[30], and one where the near edge X-ray absorption fine structure (NAXAFS) technique was employed to aid in the structure determination of various graphitic CN compositions[31,32].

CAS was also used to search for compositions of C_5N and CN containing graphite. Using the C_5N search term and aside from the original Bartlett papers and numerous hits regarding diamond-like carbon nitrides, other concepts pertaining to N-containing carbon nanotubes[33], C_5N micro-domain analysis in CN laser-ablation matrices[34], and other claims of CVD-produced CN graphitic materials[35] were also found.

The carbon-nitrogen graphite search term yielded significant numbers of references that were reviewed by title and abstract browsing. The great majority of the returned publications were dedicated to the diamond-like carbon nitrides. The extracted references pertained to those noting CN graphitic materials and those describing analysis methodologies for elucidating

structural information for less ordered nitrogen-containing carbons. Included are publications specifically addressing detailed vibration spectroscopic structural assignments[36,37,38], sources describing in-situ electron beam and X-ray techniques for observing the change that nitrogen doping induces on graphites[39,40], others demonstrating additional analytical methods not yet covered here such as mass spectrometry[41] and solid state NMR[42], proposed CN_x fullerene and nanotube structures[43,44], and additional reports of carbon nitrides[45]. Also of particular mention are publications covering computational modeling[46,47,48] of carbon-nitrogen sheet-like structures.

In comparison with extensive work done over nearly a century on studying and validating the structure of graphite[49,50,51,52] and a vast number of its intercalates[53,54,55,56,57,58], very little was found regarding the intercalation of CN_x materials. CN_x structures, including hard carbon nitrides, have been intercalated with lithium as a synonymous application to graphite in battery and capacitor applications[59,60,61], with nitric acid[62] where oxygen was incorporated into the graphite matrix, and most notably with fluorine[63] into a catalytic-CVD-derived CN_x[64,65] as it correlates closely with the well-known graphite fluorides[66,67,68]. However, even though some of the most uniform graphite and boron nitride intercalates have been produced[69,70,71,72,73] by reaction with the access-limited peroxydisulfuryl difluoride[74,75,76,77,78,79,80,81] ($S_2O_6F_2$), no reports were found where graphitic CN_x or even diamond-like carbon nitrides were interacted with $S_2O_6F_2$, a subject of the present thesis.

According to the present search, there is no evidence of any attempted purification attempts on CN_x deposits. In addition, there do not appear to be any reports of researchers attempting to elucidate the structure and bonding of the nitrogen centers by chemical modification beyond the aforementioned intercalation work. The use of detailed thermal

analysis to extract phase change information and decomposition energies has also not been reported for CN_x materials. Also, there were no reports found of actual yields or synthetic rate capabilities for the production of the graphitic carbon nitrides, a trend that is not altogether uncommon in the field of solid-state, thin-film synthesis[82,8382-83].

In summarizing the open literature in regards to nitrogen-doped graphite, it can be shown that graphite-like materials of composition C_5N have been produced independently by two separate research groups more than 15 years ago. Reproduction of these original syntheses were afforded and further optimized in the current thesis, enabling the study and comparison of the carbons of interest. Initially, it makes sense to utilize the standard X-ray and electron beam techniques covered in these earlier reports to verify composition and some structural information. Advances in analytical technology and electronics since the original work on C_5N were exploited in an attempt to extract additional information from the materials.

All of this work would be for naught without a careful definition of graphite and other states of carbon. The following discussion surrounding states and definitions of carbons is consolidated based on the text of Weiss, et al.[84] Graphite is defined as carbon arranged in a completely unsaturated and infinite sheet of 6-membered rings, arranged in lamellar format with identical sheets stacked infinitely perpendicular to the planar sheets called graphenes. The sheets, although not directly bonded to other sheets, are held close together by Van der Waals forces. As with just about any chemical crystalline substrate, perfection in perpetuity in all directions is statistically improbable and dictates that imperfections will exist. Such imperfections include but are not limited to: elemental contamination, puckering of the sheets, particulate inclusions, substituent contamination, surface exfoliation, graphene edge terminal

substituents, ring size variations, and crystal twinning zones; all of these will be present in the bulk of even the most pristine graphite samples.

Once the imperfections of a graphitic system increase in quantity and size providing a more macroscopic effect, the carbon domain is loosely defined as amorphous. The designation as amorphous indicates little more than a lack of order for any continuous domain. In fact, materials that resemble graphite structurally but have disrupted sheet spacing such as turbostratic graphites are also included in the amorphous continuum. Of even less order are those carbons deemed as graphite-like amorphous materials which cannot be structurally elucidated because of the lack of order but resemble graphite in terms of physical properties such as electrical conductivity, chemical reactivity, density, and hardness. Most graphite-like designations can be structurally associated with small and numerous graphene domains present in the structure. Once the sp^2 bonded centers give way to sp^3 bonding modalities, the material enters the continuum of hard carbons which have mixed properties of diamond and graphite. Amorphous carbons with increasing diamond characteristics are termed diamond-like. Finally, order of the diamond-like continuum increases until crystalline diamond is obtained.

The inclusion of periodic impurities into a graphite matrix produces a "graphitic" derivative at the epitome of maximum order. Similar to the terminology for amorphous carbons, continued introduction of disorder derives graphite-like materials and so on. This is the applicable basis for discussions surrounding the nitrogen-doped carbons of the current investigation. It is worthwhile to note that references to "C_5N" within this text are intended to represent the graphite-like C_5N reproduced from the reports of the 1980's.

Theory

If one wishes to make a graphite matrix more easily oxidizable, contracting the energy difference between the HOMO and LUMO levels thus better stabilizing a charge in the oxidized state it is desirable to increase the electron donor capacity of the system by incorporating electron-rich heteroatoms. Graphite represents a 2-dimensional planar network of carbon stacked in a hexagonal configuration; the substitution of a heteroatom into the matrix often dramatically affects this planarity and thus its properties. Nitrogen as a dopant is no exception to this effect; however, if ternary nitrogen in a π-conjugated system is oxidized to the corresponding nitrogen cation, it adopts the planar sp^2 hybridization and is capable of bearing charge as evidenced in the wealth of literature on N-fluorinated salts and a number of cyclic N-oxides.

This capability of a material to stabilize charge is quite important. Graphite is well known for its ability to undergo intercalation by a number of chemical moieties. One notable example is exemplified by its reaction with alkaline earth metals to effectively produce anionic graphite with the alkaline earth metals bearing positive charges. This concept has for years laid the foundation for the storage capacity known for rechargeable lithium ion batteries as it pertains to the negative electrode. Countless examples of graphite oxidation also exist as exemplified by examples such as graphite oxide and that which has been treated with $S_2O_6F_2$. However, a great majority of the cases of graphite oxidative intercalation lead to the formation of a covalent bond with the oxidant, rather than an ion pair, rendering the process irreversible.

Now imagine that nitrogen is incorporated into the graphene layers in a way that provides a general and homogeneous effect. For the purposes of this study, C_5N is presumed to fulfill this criterion on the basis that with a consistent spacing of nitrogen, any 6-membered

carbon ring unit is bonded directly to at least one nitrogen atom. If a graphene structure with 6-membered rings is presumed for the theoretical material one would expect a system possessing nitrogens on the internal portions of the sheets and those on the edge as in the pictoral representation in Figure 1[85].

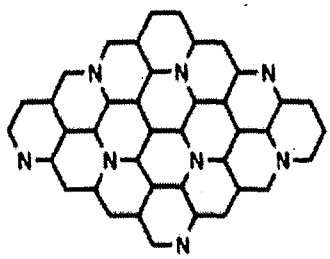

Figure 1 - Structural rendition of CxN

It becomes readily apparent that the nitrogen atoms in the central portions of this hypothetical structure should possess some sp^3 character in the neutral state and as such should not be in the plane, creating a distortion to the supposed theoretical structure. This is where oxidative rehybridization can aid in the formation of nitrogen-doped graphene. Either centrally situated or edge nitrogen environments when oxidized and bearing a charge should in theory adopt the cationic sp^2 hybridization as depicted in Figure 2; this reasoning is also extended to the unlikely neutral trigonal planar structure.

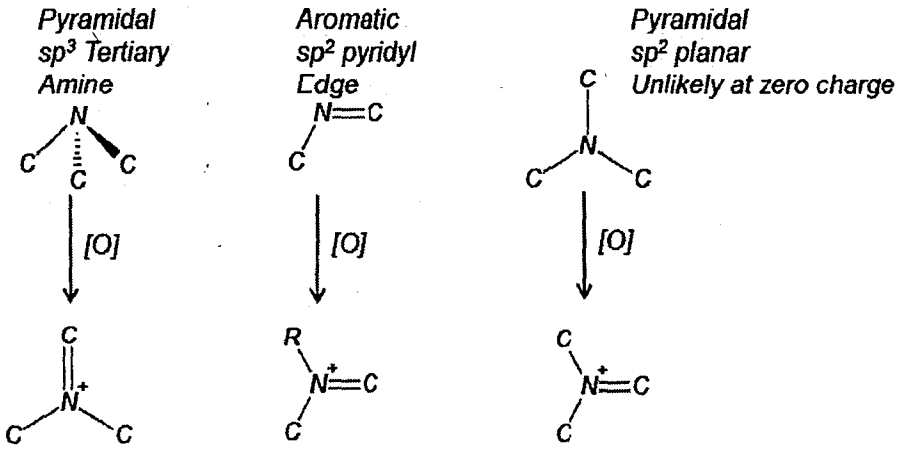

Figure 2 - Rationalization of Nitrogen Hybridization Before and After Oxidation

Once graphitic C_5N or other conjugated structure is obtained, it should feasibly be oxidizable and capable of intercalation. The originators of graphite-like C_5N in Neil Bartlett's research group[1-3,6-7] published numerous intercalation attempts and results for a plethora of graphites and graphitic material. The reasons are unknown, but the same attempts were never reported in regards to C_5N which could have shed much detail about the nature of the material. This observation forms one of the cornerstones of the current work where the carbons and carbon nitrides produced are reacted with the quintessential oxidative intercalant peroxydisulfuryl difluoride, $S_2O_6F_2$, with the aim of revealing the reactivity and potential graphitic character of C_5N.

Despite the noble attempts of previous researchers, the true structural nature of C_5N remains unsolved. One aim of the current study is to exploit the advances in electronics and instrumentation in the 20+ years since the graphite-like C_5N was last reported in the literature. While some of the original techniques used to characterize C_5N in the 1980's were repeated in this study, the quality and value of the data is considered to be greatly improved based solely on

the advanced capabilities of modern instruments. In addition, newer techniques were also used in order to gain further insights; such methods include solid state NMR, high resolution electron microscopy, electrochemical cyclic voltammetry, electron spin resonance (ESR), and thermoanalytical techniques.

Another improvement which led to a better understanding in the chemistry and preparation of C_5N is the enhanced control over reaction conditions. The original researchers were forced to use cold baths in order to control the vapor concentration of the reactants, a technique which is ingenious but troublesome because the true temperature of the bath can never be equilibrated due to the evaporation of substrate constantly cooling the medium and thus changing the reactant concentration in the vapor phase. In this study, serial dilution of static room temperature solutions of substrates can be directly measured for content by optical spectroscopy and serially diluted using very accurate flow control and mixing equipment (see Experimental section).

While direct structural characterization of C_5N was not possible as a result of randomized or poor order characteristics, additional insights can be gleaned by comparative analysis of C_5N with graphite. Anticipating the dissimilarities between C_5N and well-ordered graphite a pyrolytic carbon prepared in the same manner as C_5N was for providing a three-way comparison in regards to the affect of the nitrogen.

Results

Synthesis

The literature descriptions for the synthesis of graphite-like C_5N from Bartlett, Labes, and Shen all lacked specific details regarding absolute rates, concentrations, reactant ratios, and

yields. Given this challenge it was worthwhile repeating the synthetic optimization described by Shen. Using an updated flow system (described in greater detail in the Experimental section) pyridine vapors from a 20 sccm gas flow at 0°C were carried into a quartz furnace tube in either nitrogen or helium. By incrementally increasing the reactor temperature under flow, it was verified in accordance with Shen's thesis that pyridine is stable in the reactor alone at temperatures up to 950°C for both carrier gases where it begins to form a black tar on the cooler surfaces at the reactor exit. The FTIR of the reactor effluent also confirmed that pyridine remained unchanged in the designated temperature range proving that pyridine alone was not responsible for the formation of C_5N. The same experiment was repeated with benzene showing a decomposition onset at around 980°C.

Secondarily, it was important to optimize the reaction temperature. We knew from the review above that nitrogen content in the prepared materials is compromised by excessive temperatures, thus necessitating the lowest reaction temperature tolerable. Pyridine readily reacts with chlorine gas under ambient conditions to produce chlorinated pyridine which is sequestered as a salt by the hydrogen chloride byproduct. Accordingly, the two reactant streams were kept separate up to the heating zone of the reactor. This was accomplished by flowing nitrogen or helium at 20 sccm through dry pyridine at 0°C into the reactor through a smaller quartz inner-tube. This flow was complemented by the theoretical 5/2 stoichiometric equivalents of chlorine gas diluted in an additional 20 sccm of the same diluent gas (N_2 or He) as used for the pyridine. Starting at room temperature, the pyridine chlorination reaction was readily apparent by the instant growth of white, needle-like crystals of the chloropyridine hydrochloride salt. Small traces of HCl gas could be observed in the IR for the reactor effluent possibly arising from multiple substitution reactions of pyridine by chlorine. The temperature of

the reactor was elevated in 10°C increments. The first step change in behavior was at 120°C where the pyridinium salts inside the reactor were volatilized and redeposited on the cooler surfaces near the reactor exit. As the temperature increased, the HCl signal in the IR increased steadily with temperature. At 400°C for both carrier gases, the deposit at the reactor exit began to appear yellow which was later found to be perchloropyridine as evidenced by GC-MS analysis in chloroform. No deposits were observed in the reactor heat zone when using nitrogen as the carrier gas until the temperature of 760°C. Maximum deposition rates were observed at around 800°C, as reported as operating conditions by both Bartlett and Labes when nitrogen was used as the carrier gas. For helium, the deposition onset began at 650°C and maximum deposition was realized at 700°C as described by Shen. The product possessed a lustrous-metallic appearance as described in the literature. Under these conditions, copious amounts of HCl and traces of HCN and cyanogen were observed in the IR of the reactor effluent. The dramatic temperature difference between the onset temperatures when using the two different carrier gases can be explained by the improved thermal conductivity and kinetic transport of helium over nitrogen. Given this demonstration, helium was chosen as the carrier gas for all subsequent studies and syntheses. As shown later, this disparity in temperature effect is also an indicator of an apparent kinetic factor in the product's deposition. The procedure of optimizing temperature, flow, stoichiometry, and carrier gas was not repeated for the preparation of the benzene analog of C_5N but rather directly transferred conditions for purposes of making a direct comparison.

Following the optimization of conditions for the synthesis of C_5N, it was important to evaluate the appropriate stoichiometry of reactants, similarly to those laid out by Shen. Using the ¾" quartz reactor tube, the initial optimization was targeted toward maximum yield.

Operating at 700°C, the helium diluent flow for each reactant was kept at 20 sccm and the pyridine purge solution was held at 0°C; the chlorine stoichiometric equivalent relative to pyridine was varied from 1 to 5. In general it was found that C_5N could be deposited under all of these conditions. However, at ratio equivalents less than 5/2 chlorine/pyridine, the chloropydine-HCl salt and extensive tar depositions at the colder reactor exit were strong indications of a loss of yield; the IR analysis of the exit gases indicated only increasing HCl content as chlorine concentration increased and included traces of unreacted pyridine and hydrogen cyanide. At concentrations of chlorine greater than 5/2 equivalents per pyridine, the tar byproduct observed at the reactor exit transitioned to the crystalline, yellow perchloropyridine. Analysis of the exit gas by IR indicated no free pyridine while a steady HCl concentration and chlorine gas became apparent its UV-Vis spectrum. The 5/2 chlorine per pyridine indicates the optimum theoretical stoichiometry but in reality indicated the maximum conversion of C-H bonds as evident by the concentration of HCl observed in the gas phase without having excess free chlorine which tended to produce chlorinated impurities in the C_5N product. This stoichiometric ratio was carried throughout the synthetic regime. The optimization procedure for stoichiometric balance of chlorine to aromatic substrate was not repeated for the benzene analog. Rather, the conditions were assumed to transfer ideally so that the chlorine/benzene stoichiometric balance was changed to 3:1 in order to accurately reflect the commensurate number of hydrogens on the benzene molecule.

Using the same ¾" reactor, an increased deposition yield was realized by increasing the pyridine throughput by raising the bath temperature to 22°C and adjusting the chlorine to match the optimum stoichiometry. Under these conditions, 20-22% isolated yields of C_5N were routinely obtained, but netting only 70mg of product per run. Repeating the above optimization

procedures at the higher rates of reactant throughput led to the same conclusions and did not improve the net yield beyond the 22% listed above. The product thus obtained possessed relatively high amounts (about 3% atom-mole) of chlorine as will be discussed later in greater detail. All of the development work to this point was performed using a clam-shell furnace with a 6" heat zone. The same reaction was then carried out using a furnace of 12" in length affording double the yields ranging from 40-44% netting about 140mg of product per run. Product thus obtained was found to contain about 1-2% atom-mole of residual chlorine.

This increase in yield by doubling the reactor heat zone was originally believed to be due to increased surface area. Therefore, crossed quartz fins were placed through the length of the reactor's heated zone to affect a three-fold increase in effective surface area but only to discover that yields decreased to below 20% of theoretical. This was assigned to the effect of the volume displaced by the fins and the commensurate decrease in residence time of the reactants in the heat zone which will flow faster through the reactor because of the reduced volume.

Without varying the feed flow conditions the ¾" reactor was replaced by a 1-1/4" reactor effectively tripling the reactor radial volume and consequently the reaction's residence time. With this larger reactor diameter, a longer reaction heat zone, and optimized stoichiometry the synthetic yield was increased to 70-74% netting an average of 450-500mg of product per 8 hour run. This product was found to have less than 0.1% atom-mole chlorine which is believed to be the result of more efficient chlorine utilization. The enhanced residence time affected by a larger reaction volume has been shown to directly affect yield and based on the exclusion of surface area affects leaves few other explanations other than the concept that the deposition reaction, although conducted at exceptional temperatures is kinetically limited.

While the extension of quantitative kinetic evaluation of the C_5N synthesis is obvious, it was foregone in this study in order to assign the bulk of the focus on better understanding the chemical nature of C_5N in addition to its oxidized adduct.

In an attempt to vary the statistical probability of interconnecting nitrogen containing rings and biasing the system with sp^3 rather than pyridinic nitrogen, piperidine was used as an alternative reagent to pyridine. The reaction of piperidine with 10 equivalents of chlorine under the same optimized conditions did not result in any deposition in the reactor hot zone but rather the extensive production of a black tar on the colder portions of the reactor exit. Other alternative reagents were also used in an attempt to derive better ordered or higher yielding synthetic methodologies. These included 3-chloropyridine, 3-cyanopyridine, 2,6-dichloropyridine, and 2,6-dicyanopyridine each of which contained a pendant substituent likely to eliminate to produce a thermodynamically stable and entropically favored gas byproduct of either HCl or HCN. All of these materials are problematically solids of limited volatility, precluding their transport into the reactor by the carrier gas. This was overcome by nebulizing a solution of the precursor dissolved in the nitrogen-containing solvent, acetonitrile, directly into the reactor heat zone. All the above precursors produced C_5N but gave poor yields of less than 5% based on added substrate and barely produced enough product for elemental analysis. The cyanopyridines did produce the gaseous HCN byproduct expected at 700°C as evidenced by IR, and significant amounts of tar deposition were observed in addition to C_5N. The chlorine substituted precursors reacted in similar fashion producing HCl as a gas byproduct as observed by IR of the reactor effluent, with the same distribution of tar and C_5N formation. The poor yield can be rationalized to some extent based on the absolute hydrogen to basic leaving group (dither CN or Cl) ratio. Elemental analysis confirmed that all of the deposits possessed a

stoichiometric balance of C_5N and it is worth noting that no chlorine contamination was present in any of the products except for the dichloropyridine which contained only traces of the undesirable element. It was determined to forgo development of these novel syntheses in pursuit of generating multi-gram quantities of C_5N and characterizing its structure by analysis and chemical reactivity.

As will be discussed in greater detail in following sections, the products obtained by the ambient pressure CVD process employed in this study produced a mixture of particle morphologies as observed by electron microscopy, including lamellar graphite-like structures and soot-like spheres. An initial attempt to bias the formation of the desired lamellar morphologies was to significantly reduce concentration and throughput of the reactants to about 100 parts per million (ppm) by volume in the reactor at any given moment and reduce the flow of the carrier gases to less than 1 sccm as well. Numerous attempts at varying precursor concentrations, ratios, and temperatures failed to produce any difference in this distribution but only affected the independent size of the particles formed. It was concluded that the lamellar structures are formed on surfaces while the spherical particles generated in the gas phase by the same reaction and subsequently deposited at the surface. It seems reasonable that the distribution of the morphologies remain unaffected with any changes because the reactants can combine in the vapor space or at the surface in the same ratio regardless of concentration or flow. In order to overcome this, a surface-specific reaction/deposition would be required as is often employed in vacuum CVD operations and catalytic point growth mechanisms, both of which are not possible given the reaction enthalpy driving force for the system currently under study.

One final set of experiments toward the preparation of the most pristine C_5N sample were done to remove contaminant chlorine or undesirable particle morphologies. The first attempt was based on flotation of particles in a tuned density mixture of bromoform and chloroform; separation was unsuccessful. The solid products were also treated with room temperature and refluxing solvents including acetonitrile, dimethylsulfoxide, N,N'-dimethylformamaide, and N-methylpyrrolidinone resulting in absolutely no extraction of soluble solids or chlorine containing species. Thermal annealing of the product at temperatures greater than 760°C for long periods of time induced some removal of chlorine as evidenced by TGA-IR analysis but it was in the form of ClCN and was accompanied by traces of HCN, cyanogen and HCl indicating a net loss of nitrogen in excess of chlorine removal. At temperatures above 500°C a reaction with hydrogen gas induced chlorine removal but was also accompanied by significant loss of nitrogen in the form of HCN gas. The addition of excess pyridine at 700°C induced chlorine reduction in the product but enhanced the hydrogen content to undesirable levels. Treatment of the solid with lithium deuteride, butyllithium, methyllithium, and cyclohexylmagnesium bromide also significantly compromised the nitrogen content of C_5N while eliminating chlorine except in the case of the Grignard reagent for which only nitrogen was removed. These latter reactions have led to the conclusion that C_5N as produced in this work is reductively unstable and possibly indicating why the work of so many researcher to make highly ordered C_xN with high nitrogen contents by metal-catalyzed CVD were unsuccessful since many of them produce ammonia or hydrogen as byproducts.

In summary of all of the synthetic methods tested here, it was decided to proceed with the synthesis as modified from the reports of Bartlett and Labes. Net yield and overall yield

were optimized to an acceptable level and the reduction of chlorine contamination was realized in the process of driving to higher yields and thus better chlorine utilization.

In order to provide a thorough description of the best selected conditions for this investigation that is also the basis for the bulk preparation of C_5N, they are reiterated here for completeness; a more thorough description of peripheral equipment can be found in the Experimental section. Using a 1-1/4" diameter quartz furnace tube and a tube furnace with a 12" long heat zone, pyridine and chlorine were reacted to deposit C_5N on a repeated basis at 700°C. Pyridine was introduced into the reactor by passing helium gas at 20 sccm through a solution of the liquid at 22°C; since the lab temperature was continuously above 25°C there was no risk of reactant condensation which could change the vapor concentration of pyridine. Chlorine was introduced at 5/2 the stoichiometric balance of pyridine and was diluted in a second stream of helium at 20 sccm before being carried to the reactor. The deposition was allowed to continue for 8 to 10 hours followed by collection of the cooled product in air.

The benzene derived analog material was prepared in as similar a manner as possible. For comparative reasons, it was deemed important to maintain the same vapor concentration of precursor as used in the C_5N synthesis. Since benzene is considerably more volatile than pyridine, its method of introduction to the carrier gas was slightly modified. To accomplish this, helium was passed through liquid benzene at a rate of 7.8 sccm. This stream of gas was further diluted with 12.2 sccm of additional helium before entering the reactor. The ratio of chlorine to benzene was modified to 3:1 now reflecting the $C_6H_6 + 3\ Cl_2 \rightarrow 6\ C + 6\ HCl$ reaction stoichiometry. Otherwise, the conditions were identical.

Additional details on each of the synthetic developments and endeavors can be found in the Experimental Section of this work.

C5N Characterization and Comparison

The critical analysis of C_5N as produced in this study has confirmed some aspects of the previous literature and brought to light some different or interesting observations. The analyses described here were performed on material provided by the optimized synthetic process.

One of the simplest and potentially introspective analyses of modified materials is usually possible using vibrational spectroscopy. However, black-body materials such as the pyrolytic carbons derived from this study do not offer themselves simply to analysis by reflective surface IR spectroscopy or transmission spectroscopic methods. Both of these methods were tried on film and powder samples with no observable signals. High pressure attenuated total reflectance-FTIR analysis of C_5N on a diamond anvil press enabled very weak duplicate spectra to be obtained as seen in Figure 3 from the same sample pressed twice for analysis.

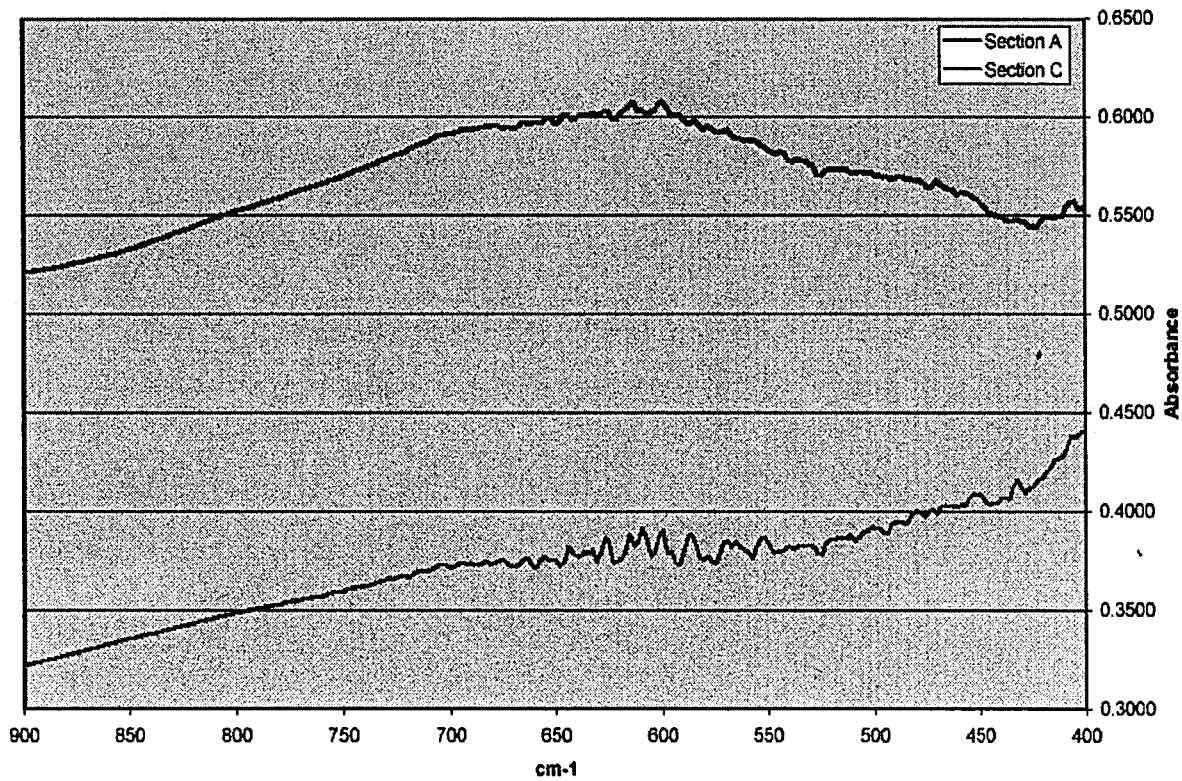

Figure 3 - ATR-FTIR spectrum of C_5N

It is difficult to discern any distinct vibrations in relation to CN moieties but there are weak signals observed in the low frequency region that coincide with graphitic planar deformations. In light of this result, the benzene analog to C_5N and pure graphite were not comparatively analyzed by this method.

Because of the scattering nature of confocal Raman spectroscopy, it does however offer the ability to analyze the surfaces of black bodies. The Raman spectra of C_5N obtained from the various synthetic conditions showed no significant differences. In general, the spectrum of C_5N, shown in Figure 4, was very weak but does show broad bands for the G and D vibrations of graphite-like carbons. The weak signal, broadness, and lack of intensity difference for the G and D bands indicate a relatively amorphous material[86].

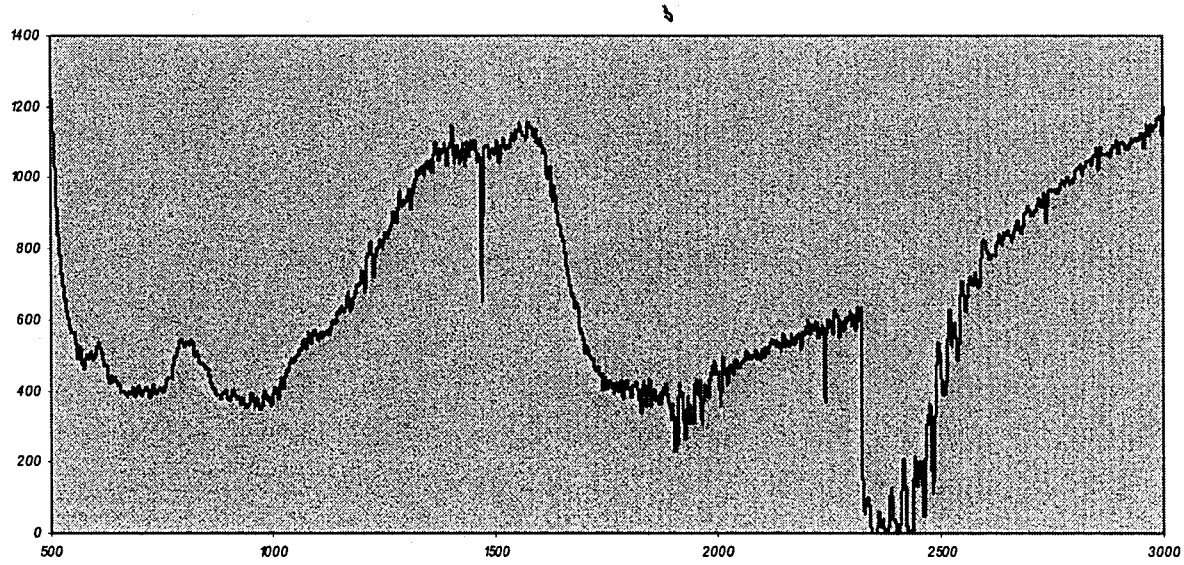

Figure 4 - Raman spectrum of C_5N

It is reasonable to expect that the symmetry of the normal vibrational modes of graphite would be seriously disrupted by the nitrogen substituent giving rise to spectra of poorly ordered materials, thus the Raman spectrum of the benzene analog to C_5N was obtained as shown in Figure 5.

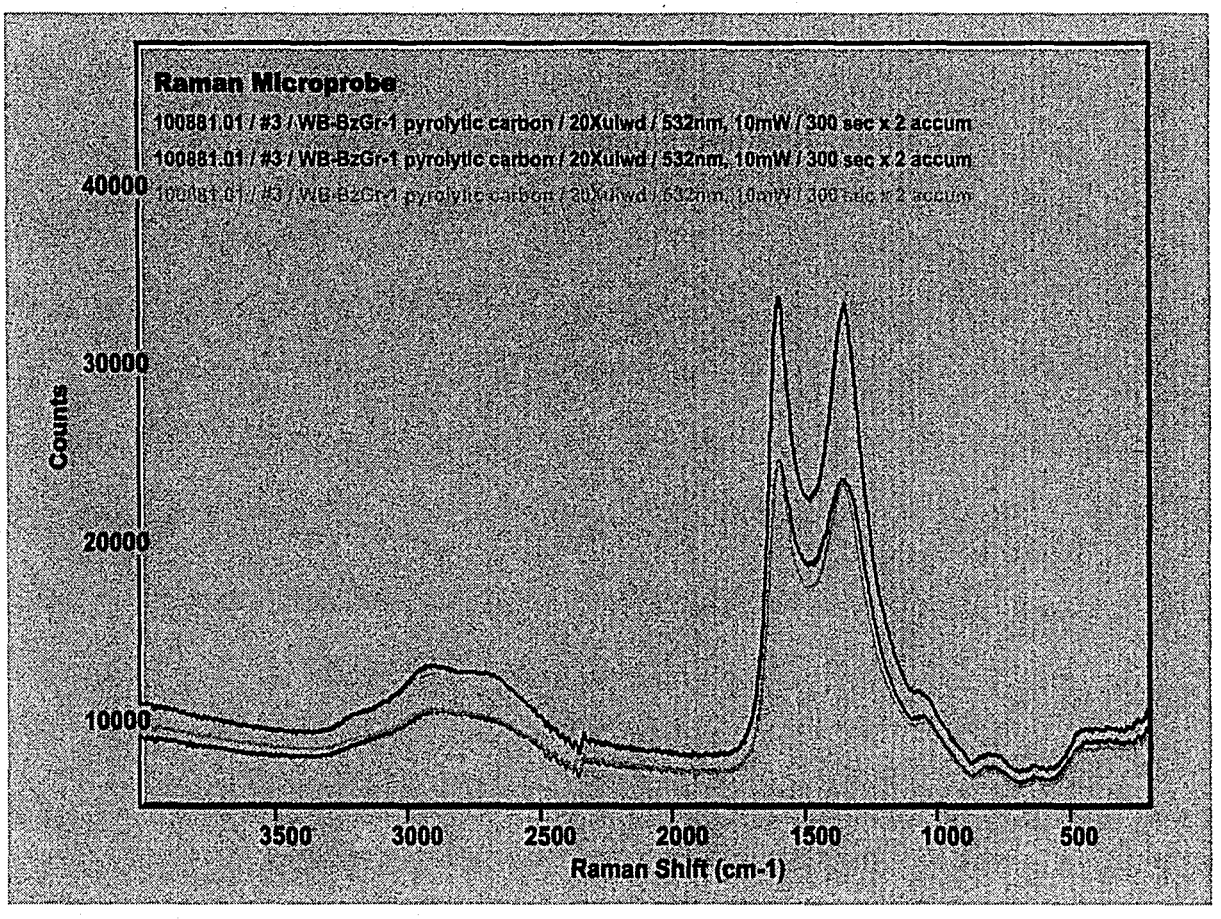

Figure 5 - Raman Spectrum of Benzene Derived Analog of C_5N

The apparent improved signal intensity and line sharpness of the G and D bands of the benzene analog relative to C_5N supports the idea that nitrogen distorts the order and symmetry of the vibrational modes of a graphite-like material, assuming that the materials are structurally similar. The ratio of the bands for this analog, however are indicative of a highly amorphous material. A comparison to graphite and amorphous carbon soot is provided in Figure 6. The sharp features, high intensity, and peak ratios of the G and D bands all indicate a relatively high quality graphite material while the soot spectrum resembles that for the benzene analog discussed above.

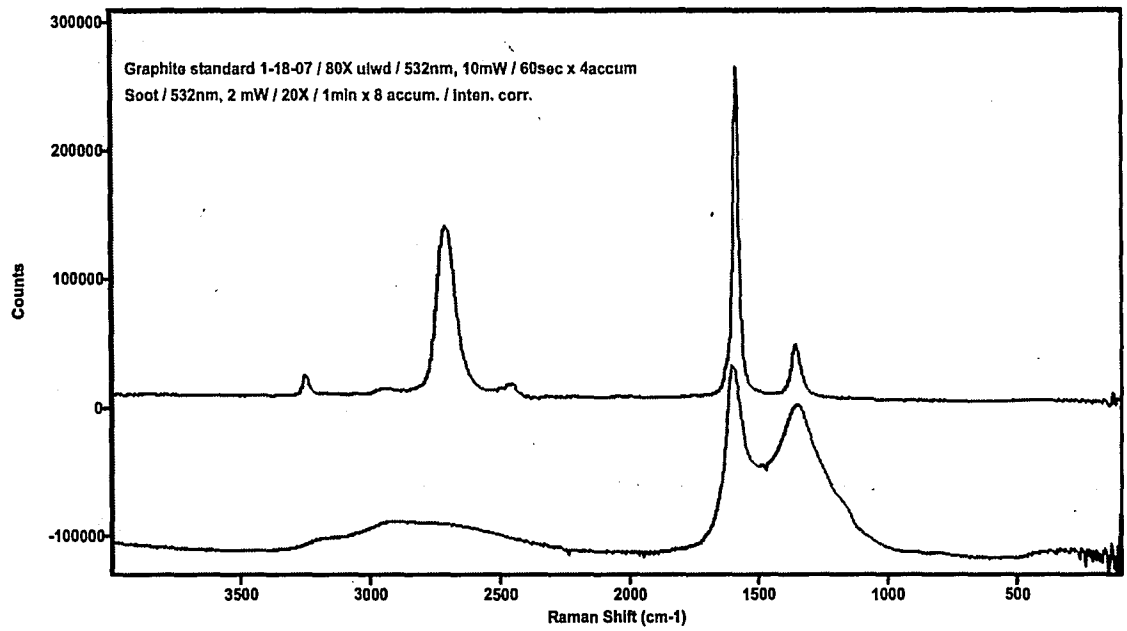

Figure 6 - Raman Spectra of Commercial Graphite (top) and Amorphous Carbon (bottom)

In summary, the vibrational spectrum of C_5N indicates that it is highly amorphous but with the desirable sp^2 hybridized features of a graphite-like material. None of the observed spectral bands indicate the presence or nature of the entrained nitrogen.

Another analytical measure of order and function is X-ray diffraction (XRD). C_5N continues to display poor ordering characteristics as seen in its powder XRD pattern (Figure 7). Two broad features show lattice spacing consistent with those of graphite. The broadness and reduced intensity of this spectrum indicate either a very limited amount of order or order on a micro-crystalline basis. The d-spacing of 3.6-3.7 angstroms coincides with the graphitic inter-planar spacing.

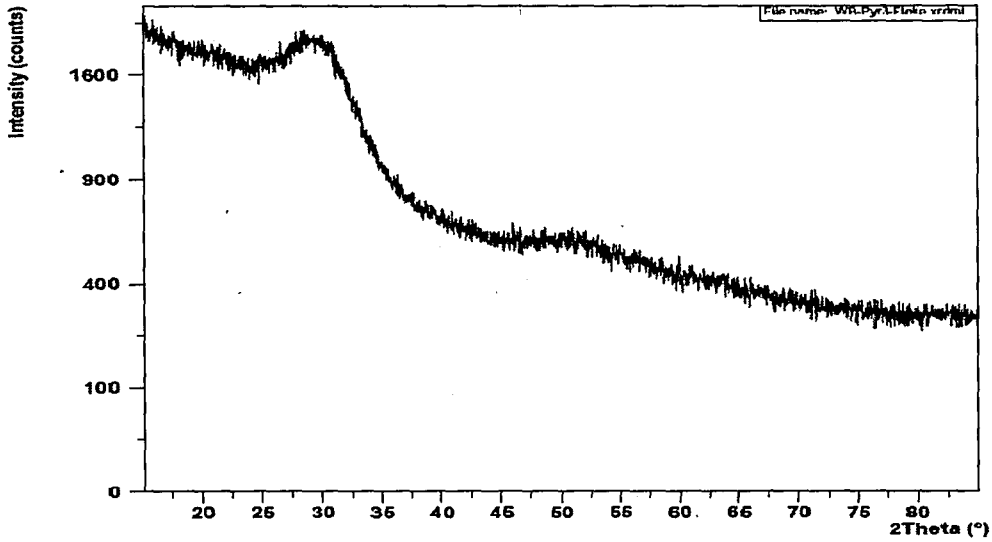

Figure 7 - XRD of C_5N

The benzene analog also produces a weak XRD pattern as displayed in Figure 8. This continues to confirm the poor ordering of materials produced by low temperature pyrolytic condensation.

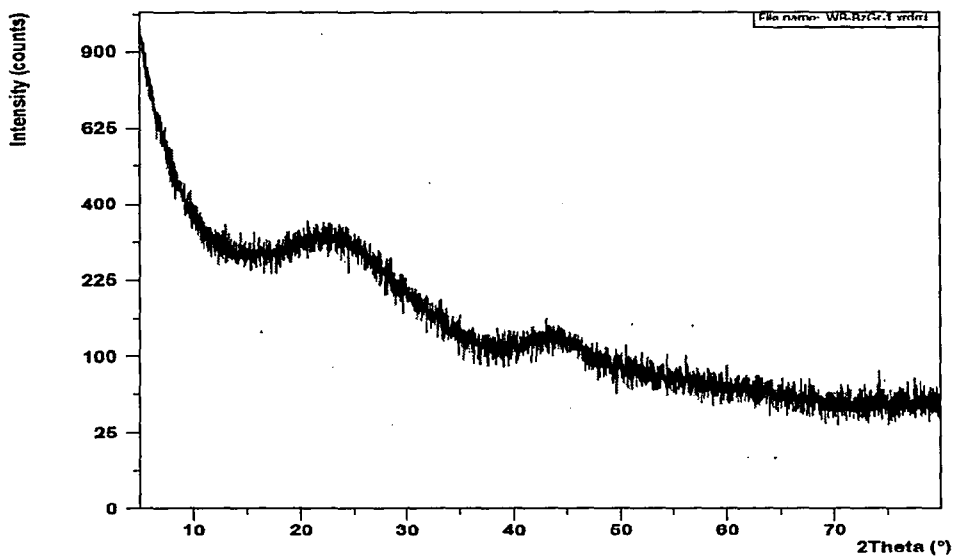

Figure 8 - XRD of Benzene Analog to C_5N

In stark comparison, the XRD of a graphite standard displays more considerable detail as seen in Figure 9, showing strong, sharp features of a well-defined crystalline matrix with pristine interlayer spacing.

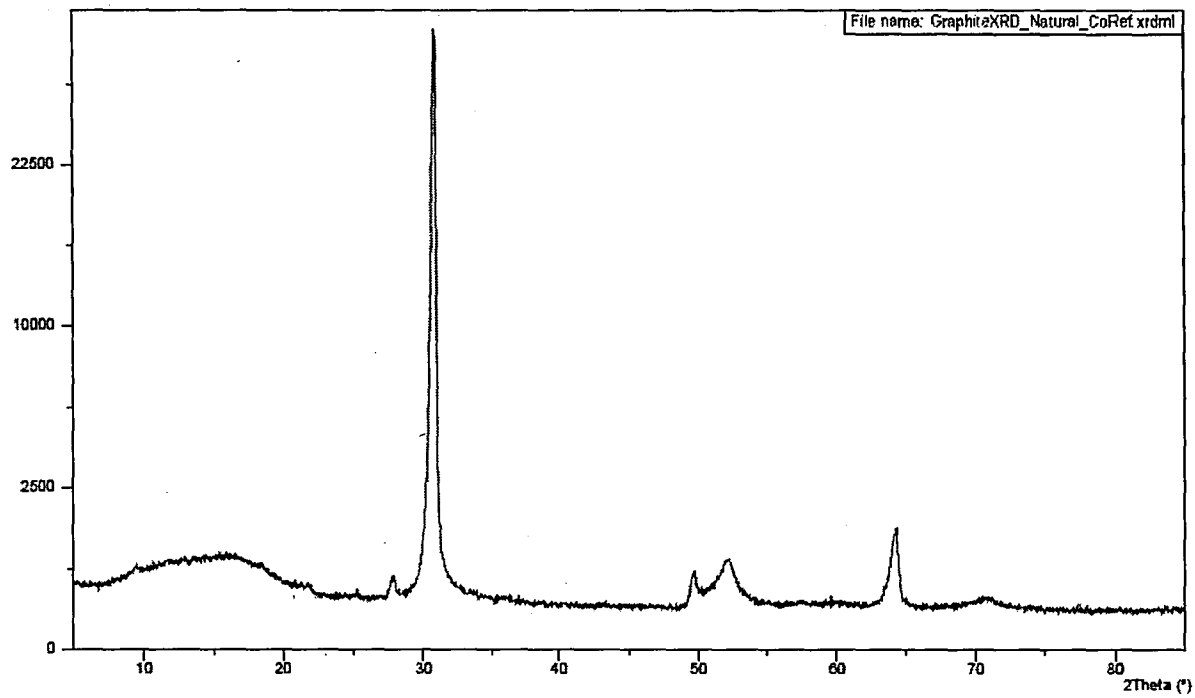

Figure 9 - XRD of Graphite Standard

X-Ray photoelectron spectroscopy (XPS) coupled with electron spectroscopy for chemical analysis (ESCA) is a method for validating the elemental composition and chemical environment for atoms near the surface of a substrate. Both films and ground powders gave similar results for C_5N at the surface and ESCA confirmed the C_5N composition but also indicated the presence of chlorine as discussed earlier. Sputtering into the surface in order to ascertain homogeneity caused damage to the specimen in the form of nitrogen loss as confirmed by bulk elemental analysis; this point appears to have been missed in Shen's thesis as he concluded that nitrogen content actually decreases as the surface is penetrated with ion sputtering. Oxygen was observed in the ESCA analysis of all materials in this study. The carbon and nitrogen

environments in the XPS spectrum shown in comparison with graphite in Figures 10 and 11, respectively, indicate graphite-like sp^2 hybridization and reduced order as seen in the broad features of the C1s binding energies. The N1s shows two distinct regions of binding energies assigned as a distorted tertiary-amino sp^3 at 401 eV and pyridyl sp^2 at 397 eV in nearly equal amounts.

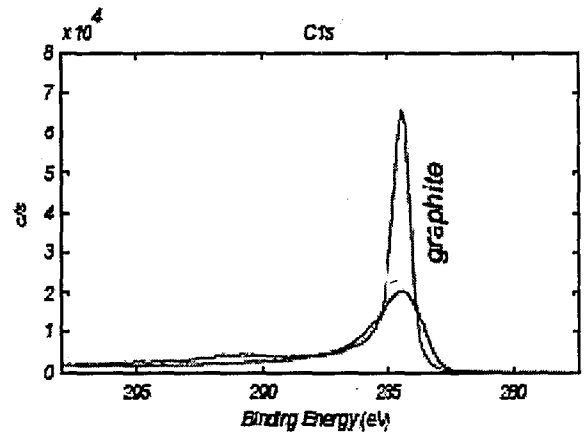

Figure 10 – XPS C1s Region of C_5N (broad) Compared with Graphite (sharp)

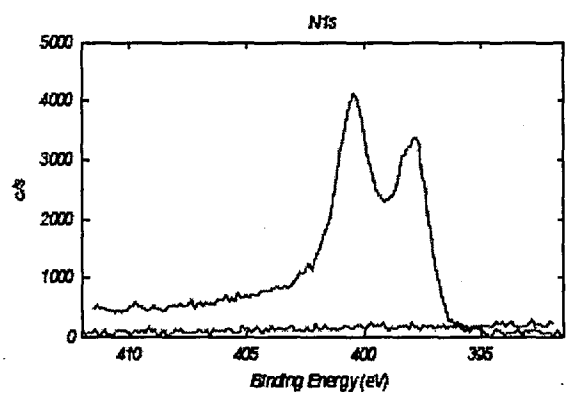

Figure 11 – XPS N1s Region of C_5N (signal) Compared with Graphite (baseline)

This 1:1 ratio of pyridyl to amino nitrogen sites is quite different from that reported by Shen at nearly a 1:5 pyridyl/amino comparison. There may be several explanations for this. One concept to consider is that the synthesis employed in this study produced smaller domains or

more defects with increased edge sites. Another explanation may be that modern equipment enables a deeper analysis into the sample surface giving a much broader representation of the material. Assuming that pyridyl nitrogen atoms represent sheet edges and amino nitrogens represent internal sheet placement, a 1:1 ratio of each would limit sheet size from 5-12 pyridine equivalent units per sheet assuming that the sheet bears a 2-dimensional proportional balance and allowing for random orientation of the nitrogen atoms. These would be considered very small domains and would give an explanation to the extensive lack of order described thus far for C_5N.

The benzene analog to C_5N also displays a broad, graphite-like C1s band as seen in Figure 12 and is also consistent with a disordered material.

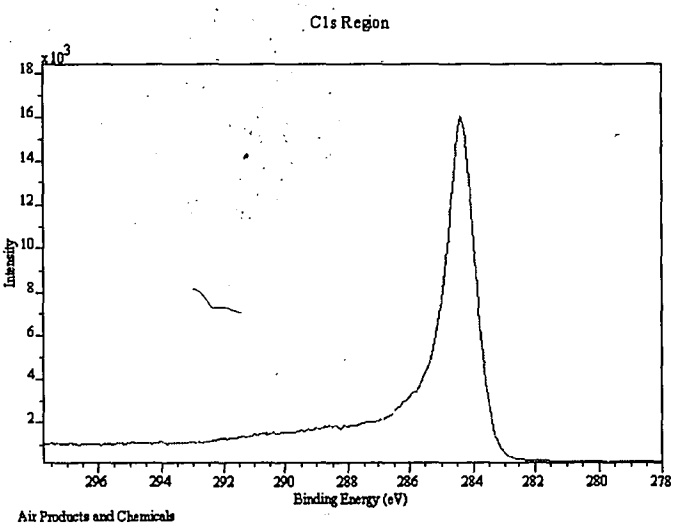

Figure 12 – XPS C1s Region of Benzene Analog of C_5N

Of course, chlorine was not observed for the graphite standard but was present in both C_5N and its benzene analog. Figures 13 and 14 show the Cl2p XPS spectra of each indicating two chlorine environments bonded to carbon; the signal at 202 eV appears to be consistent with sp^3 hybridized or internal sheet bonded carbon while its complement at 200 eV primarily indicates chlorine bonded to aryl units or to the edge of a sheet. The quantitative ratio of internal to edge

for each is very similar, 1:3 respectively. This number is not used in similar fashion as nitrogen to determine sheet size as too many unreasonable assumptions must be made in order to do so. Both materials also show a small signal at approximately 195 eV which coincides with chloride ion, a phenomenon that currently raises no explanation except for the possibility of trace contaminants such as metals or silicon, none of which could be detected directly by XPS.

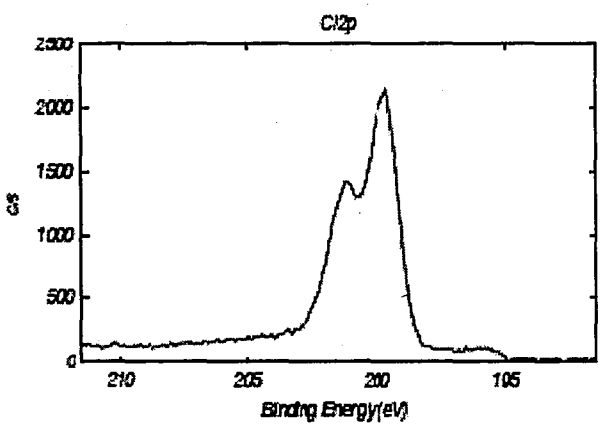

Figure 13 – XPS Cl2p Region for C_5N

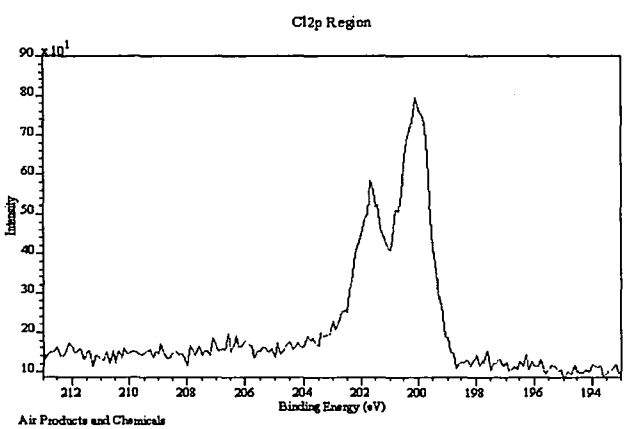

Figure 14 – XPS Cl2p Region for the Benzene Analog

It is noted that the chlorine content for C_5N obtained from the optimized synthesis is relatively low at less than 0.1% mole as opposed to the benzene analog which possessed nearly 1% mole of chlorine. Neither group originally reporting these materials in the 1980's indicated the nature of the chlorine contaminants as described here.

Closely following the ESCA results, it was necessary to validate the surface analysis with bulk elemental composition analysis for both C_5N and its benzene analog (graphite was not analyzed). Table 1 below shows the comparison of elemental composition for each material bearing in mind that only C, H, N, and Cl analyses were obtained of which the balance is assumed to be represented by oxygen.

Table 1 - CHN & Cl analysis of C_5N and Its Benzene Analog

Product	% mol C	% mol H	% mol N	% mol Cl
C_5N	76	1.1	18	0.2
Benzene Analog	90	Not detected	1	4

This confirms the bulk empirical formula of C_5N and agrees reasonably with XPS results. Also consistent with the XPS comparisons is the significant difference in chlorine content between the two species. It may be reasonable to conclude that benzene condensation is kinetically more limited than pyridine and may have required additional synthetic optimization to enable more efficient use of chlorine as was found for the C_5N case. This could possibly be the subject of a future study.

Additional insight into the prepared materials was also obtained by scanning electron microscopy (SEM) with simultaneous energy dispersive spectroscopy (EDS). Both C_5N and its benzene analog show a mixture of two different morphologies. The prominent and more desirable morphology is the lamellar or plate-like structure that resembles graphite as shown in Figures 15 and 16 for each. For both samples, these plate-like particles represent about 75% of the observed morphologies.

Figure 15 - SEM Micrograph of C_5N Lamellar Structure

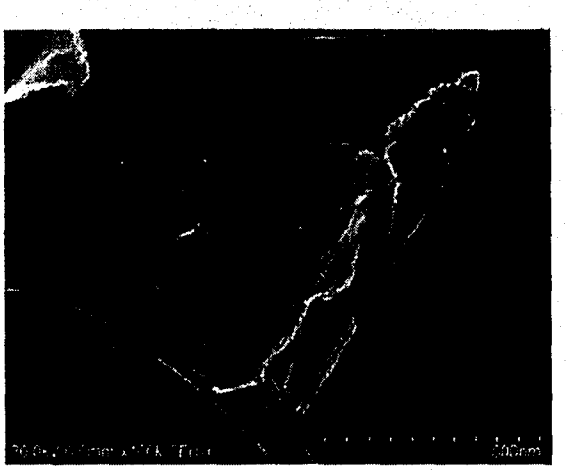

Figure 16 - SEM Micrograph of the Benzene Analog Lamellar Structure

The EDS spectra of each of these particles are as they appear in Figures 17 and 18. The nitrogen signal for C_5N cannot be resolved as it appears only as a very weak signal on the shoulder of the carbon peak. Chlorine is observed for the C_5N lamellar structures but not for the benzene analog which is unexpected based on the elemental composition analyses already discussed. The metal content in the benzene analog are attributed to focal devolution picking up scattering from the support grid.

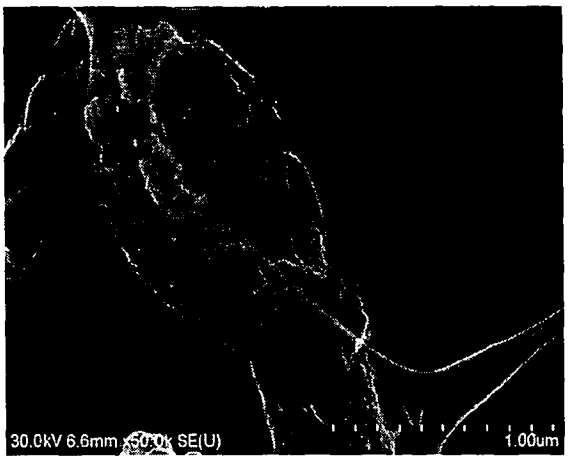

Figure 15 - SEM Micrograph of C_5N Lamellar Structure

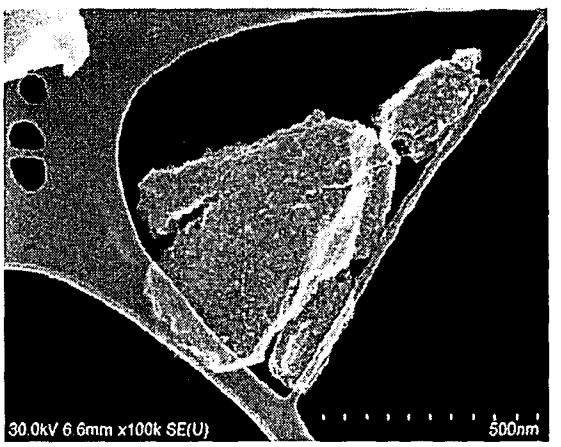

Figure 16 - SEM Micrograph of the Benzene Analog Lamellar Structure

The EDS spectra of each of these particles are as they appear in Figures 17 and 18. The nitrogen signal for C_5N cannot be resolved as it appears only as a very weak signal on the shoulder of the carbon peak. Chlorine is observed for the C_5N lamellar structures but not for the benzene analog which is unexpected based on the elemental composition analyses already discussed. The metal content in the benzene analog are attributed to focal devolution picking up scattering from the support grid.

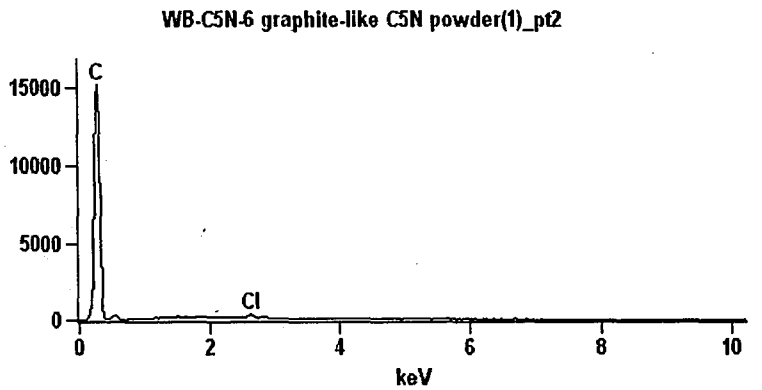

Figure 17 - EDS of Lamellar Structure of C_5N

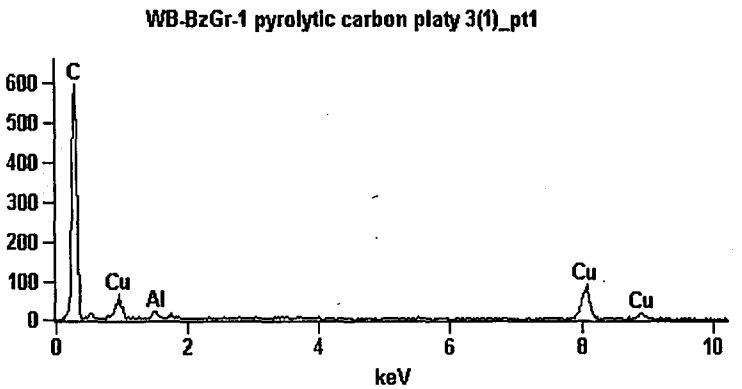

Figure 18 - EDS of Lamellar Structure of Benzene Analog

The second morphology observed in both cases is a soot-like spherical particle as in Figures 19 and 20. These represent nearly the balance of the particles observed for both condensation products. Neither of the original authors described the presence of such morphologies in their materials. They were seen in all products obtained throughout the synthetic optimization process and did not change in relative quantity with varying conditions (most likely a result of operating at atmospheric pressure).

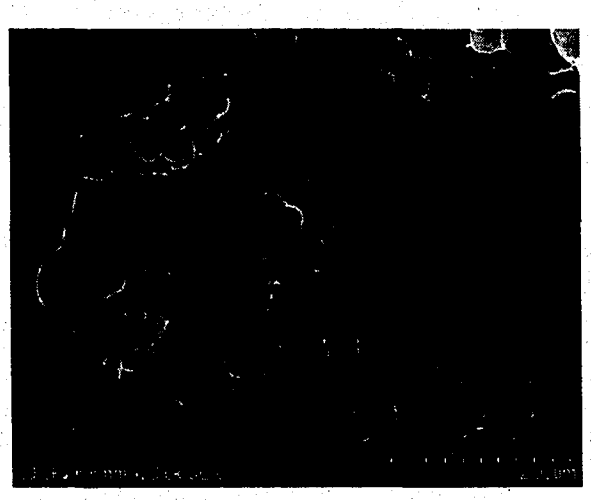

Figure 19 - SEM of Soot Particles of C5N

Figure 20 - SEM of Soot Particles the Benzene Analog

It is hypothesized that these spherical particles are formed and propagated in the vapor phase while the plate-like materials more likely grow on a surface. As already discussed, attempts to separate materials these two morphologies was unsuccessful.

The EDS spectra of these spherical materials are displayed in Figures 21 and 22. Bearing in mind that it is important to be cautious when drawing quantitative conclusions from EDS, it does appear that chlorine content in the spherical particles is higher than those of lamellar structure. This may support the concept that they are formed and propagated in the vapor

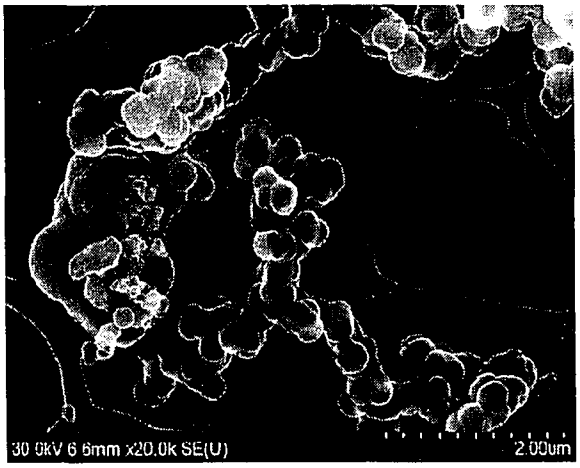

Figure 19 - SEM of Soot Particles of C5N

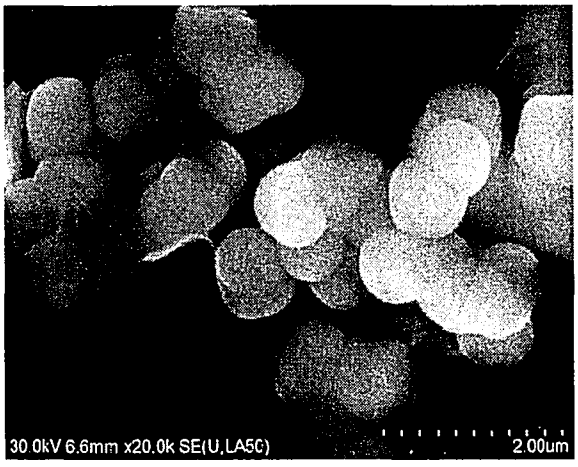

Figure 20 - SEM of Soot Particles the Benzene Analog

It is hypothesized that these spherical particles are formed and propagated in the vapor phase while the plate-like materials more likely grow on a surface. As already discussed, attempts to separate materials these two morphologies was unsuccessful.

The EDS spectra of these spherical materials are displayed in Figures 21 and 22. Bearing in mind that it is important to be cautious when drawing quantitative conclusions from EDS, it does appear that chlorine content in the spherical particles is higher than those of lamellar structure. This may support the concept that they are formed and propagated in the vapor

phase where the chlorine reactant is likely to be more abundant than at the surface where the plate-like structures are more likely to grow.

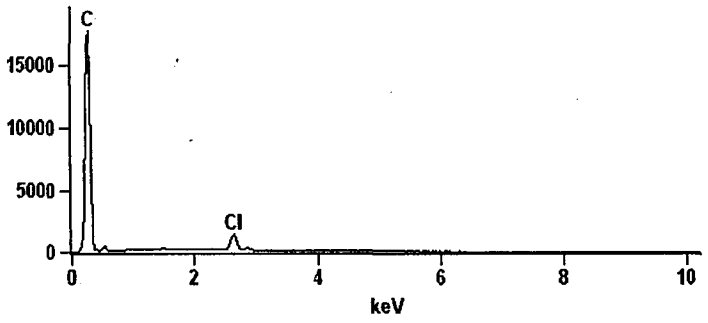

Figure 21 - EDS of Soot-like C5N

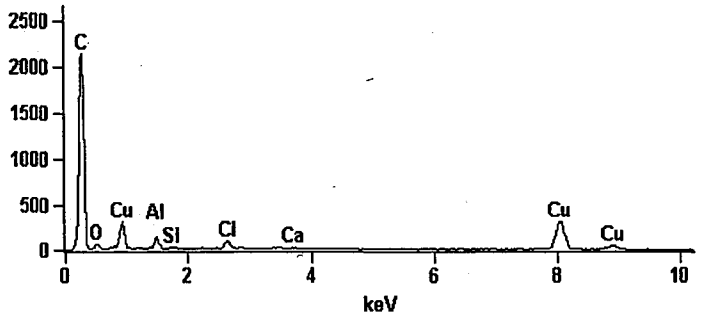

Figure 22 - EDS of Soot-like Benzene Analog

At this point it is presumed that these spherical particles are 3-dimensional solids and are not hollow based on the concept that fragments of these spheres are not observed and that multiple attempts at their microtomy were unsuccessful.

Obtaining additional structural and morphological information using SEM is not practically feasible, so the samples were further studied using high-resolution tunneling electron microscopy, or HRTEM. C_5N was observed at high resolution as shown by the micrograph in Figure 23.

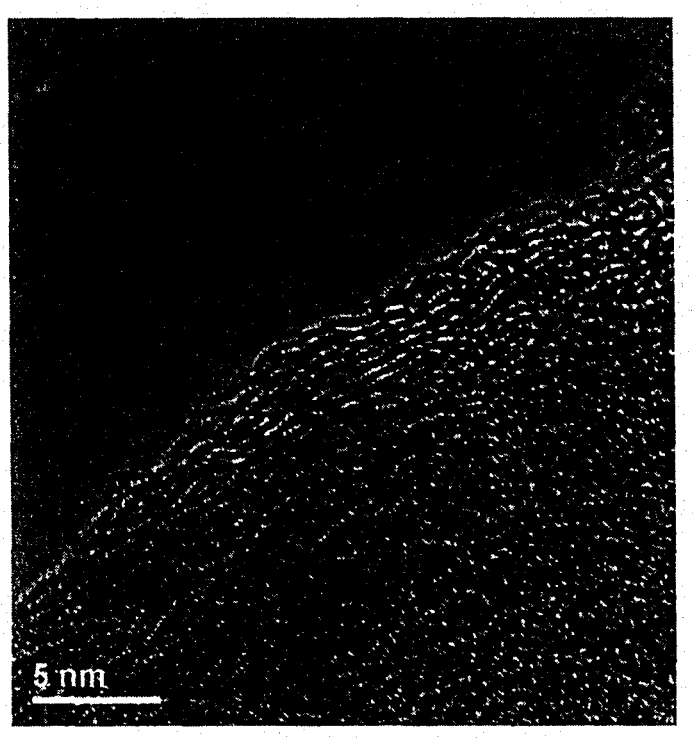

Figure 23 - HRTEM of C_5N

This micrograph shows a material that is largely amorphous although some layers and molecular sheeting can be observed indicating some graphitic character. It is important to note that all of the particles observed under high magnification appeared lamellar in nature and did not present the spherical morphology that was seen in the SEM. Also, none of the observed particles displayed diffraction behavior or fringes indicating the consistent amorphous nature of the material at hand.

The benzene analog HRTEM displayed in Figure 24 shows similar traits to that of C_5N confirming the amorphous products derived from the synthetic methods employed. This edge feature at a slightly reduced resolution is representative of both materials, showing no evidence of long-range stacking or scattering features indicating at best the presence of very small crystalline domains.

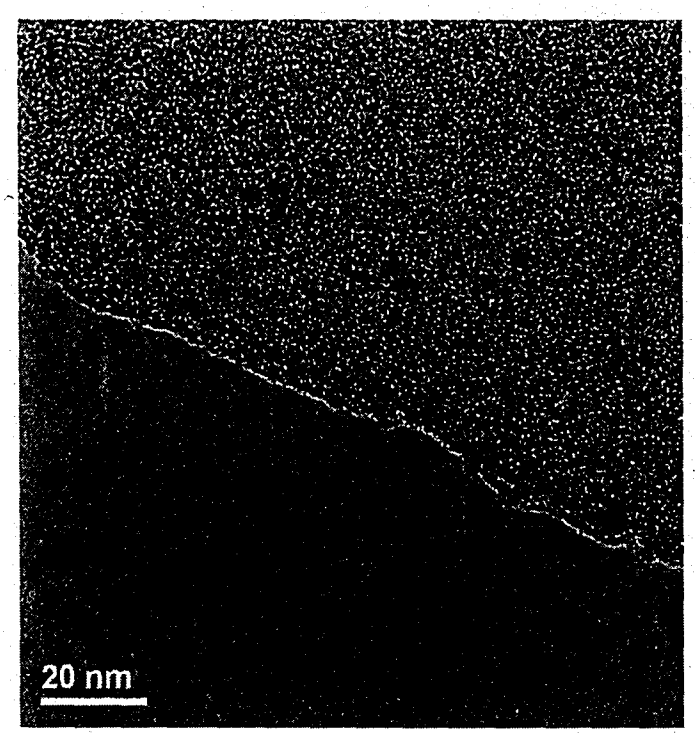

Figure 24 - HRTEM of Benzene Analog

The magnitude of disorder in the these samples is brought into sharp contrast when compared to the remarkable regularity observed in pristine, crystalline graphite as reported in the literature[87] and reproduced in Figure 25.

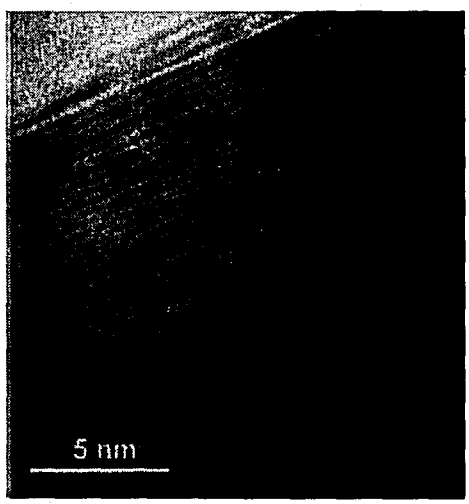

Figure 25 - HRTEM of Graphite

Electron energy loss spectroscopy, or EELS, was also performed during the HRTEM experiment in order to provide additional information. The peak position in EELS does not reveal much about materials other than the identity of an individual element and is not helpful in quantitative determinations. EELS can, however, reveal some electronic characteristics about a material based on the shape, intensity, and broadness of the spectrum. The EELS spectra of C_5N flakes displayed in Figures 26 and 27 were acquired at particle edges where the zero loss peak intensity relative to the nitrogen and carbon edges indicates the correct thickness of the sampling area. These spectra are representative of multiple sampling sites.

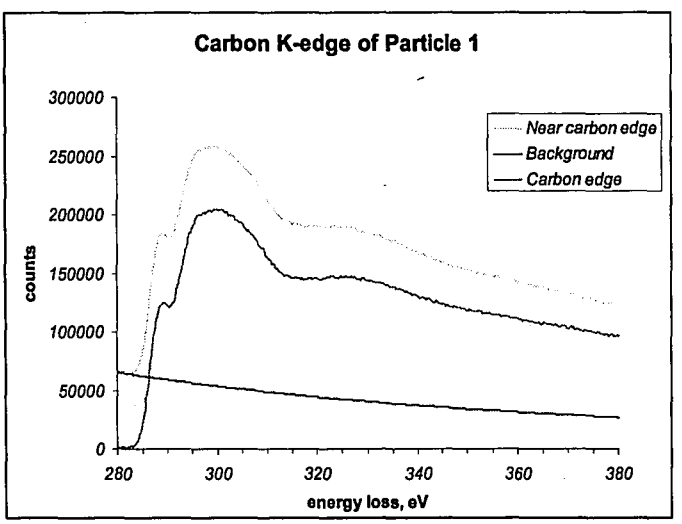

Figure 26 - EELS spectrum of C_5N Carbon K-edge

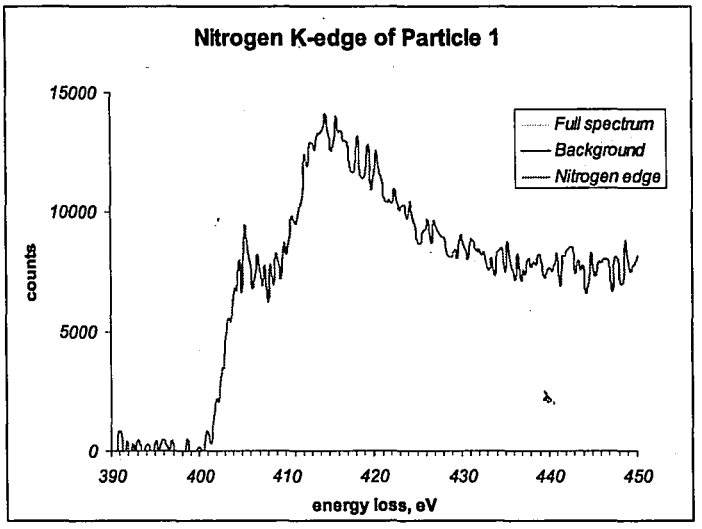

Figure 27 - EELS spectrum of C_5N K-edge

Both of these spectra show very broad σ-σ* transitions indicating a suppressed conduction band and thus reduced order as compared with graphite. Both also show a prominent and somewhat broadened π-π* transition at the lower energy indicating a modest participation of the π electrons in a delocalized bonding system. Figure 28 shows for comparison, the EELS spectrum of the carbon-edge for the benzene analog to C_5N. It is relatively similar to that of C_5N with the exception that the π-π* transition appears to be somewhat shifted and diminished possibly due to reduced conductivity of the sample that may be a result of the relatively high chlorine substitution that in theory would disrupt aromaticity. The chlorine edge could not be observed for either sample.

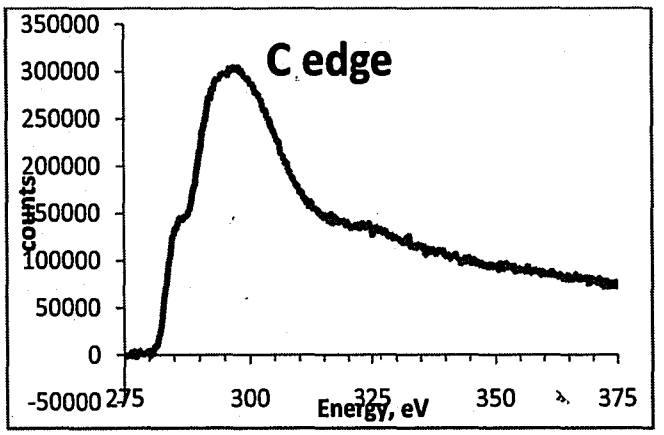

Figure 28 - EELS Spectrum of Benzene Analog Carbon K-edge

The EELS spectrum of graphite as known from the literature[88] displays a significant π-π* transition shifted to lower energies owing to the conduction band of the highly ordered material. The main σ-σ* transition is represented by a very sharp peak spanning only 10 eV. From this comparison, one can conclude that the CVD materials obtained in this study should display suppressed conductivity as a result of extended and overlapping aromatic structures.

This conductive behavior was confirmed for films deposited for both C_5N and its benzene analog by measuring conductivity using a 4-point probe. As the inverse of conductivity, sheet resistance was measured for C_5N and was consistent with that reported by Shen at 300 Ω. Commensurate with the EELS determination the benzene analog to C_5N displayed a higher resistance 460 Ω. The literature[89] sheet resistance value of graphite is 47 Ω. This comparison further demonstrates the disrupted order of the materials prepared in this study as a result of reaction conditions and possibly due to bonded elemental impurities including chlorine. Cleaning of the surface of the films with solvents reduced the conductivity values by about 5-10% indicating either contaminating of the surface with impurities or by the removal of doping impurities, none of which could be detected by evaporation of the wash liquids as described in the experimental section.

The conductivity in graphite is made possible by singly occupied molecular orbital conduction bands. Electron paramagnetic resonance (EPR, or Electron Spin Resonance/ESR) of C_5N was performed in order to evaluate the material for evidence of such a conduction band. The spectrum in Figure 29 clearly indicates that C_5N truly possesses unpaired electrons. Many amorphous carbons produce EPR signals that are due to open radical sites of stabilized radicals rather than associated with conduction bands. We can see that C_5N's EPR signal is due to a true conduction band because of its shift from the free electron g-value of 2.0023 to a smaller number of 1.9983 in addition to the dysonian line shape which is a certain sign of a true conductor[90]. The original tactic of the EPR work was to use the line shape, intensity, and broadness to estimate the actual size of graphitic sheet domains[91]. It was discovered in the process, however, that in order to use the known correlations it is imperative to account for all of the carbon in the sample gravimetrically and in the EPR. This was not possible because it became apparent that not all domains in the sample were conductive and the attempt was abandoned. This experiment did, in contrast, confirm the graphite-like conductivity that is desirable for truly nitrogen-doped graphite. A more highly ordered material would provide a most interesting future study for EPR analysis. Due to lack of accessibility, cost, time, and the inconclusive nature of the results for C_5N the EPR spectra of the benzene analog and graphite were not pursued.

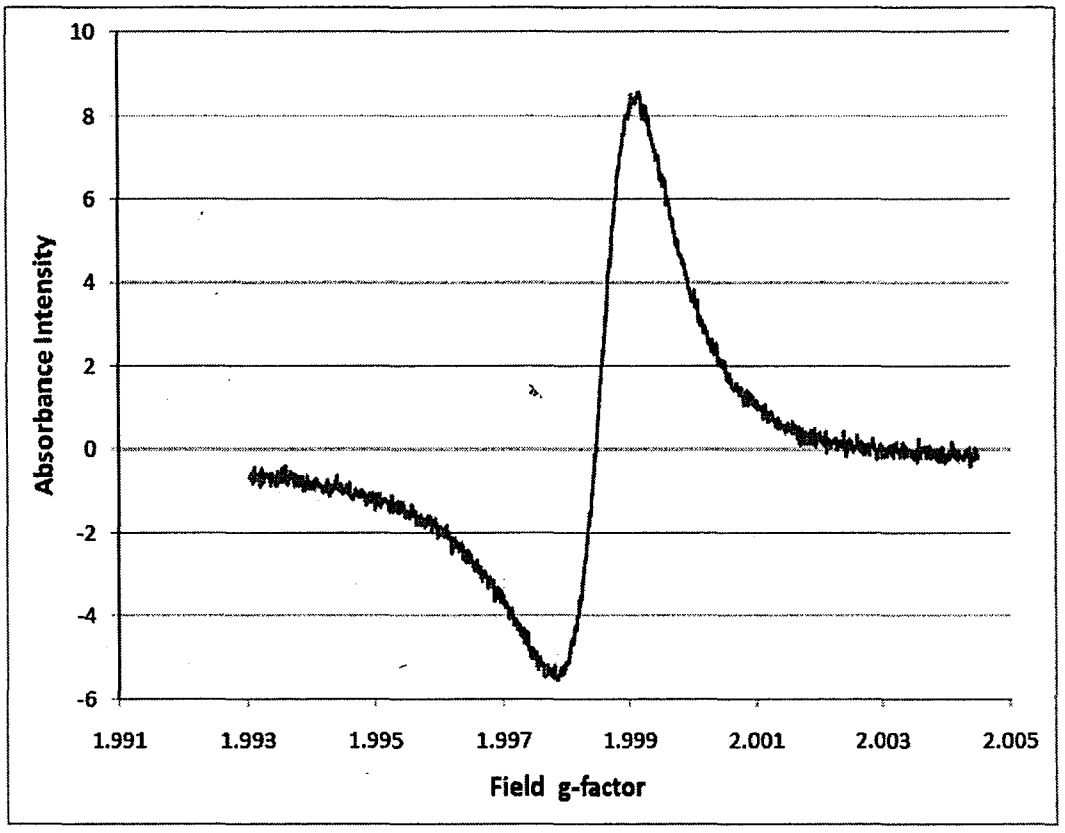

Figure 29 - EPR Spectrum of C_5N

Solid state NMR analysis has only become a mainstream method in recent years and was not previously performed with C_5N or any of the materials similarly produced. One potential problem with the analysis of the materials considered in this investigation is that they are all conductive and could possibly induce damage to the instrument by causing electrical arcing during magnetic pulse sequences. Another concern was that the paramagnetism of the materials may preclude seeing any signals. Very small samples were used to avoid the former problem. As presented here, signals were obtained including for that of the highly conductive, crystalline graphite. Figure 30 displays the stacked ^{13}C-NMR spectra of ^{13}C-enriched commercial amorphous carbon, commercial natural graphite, commercial synthetic graphite, C_5N, and its benzene analog.

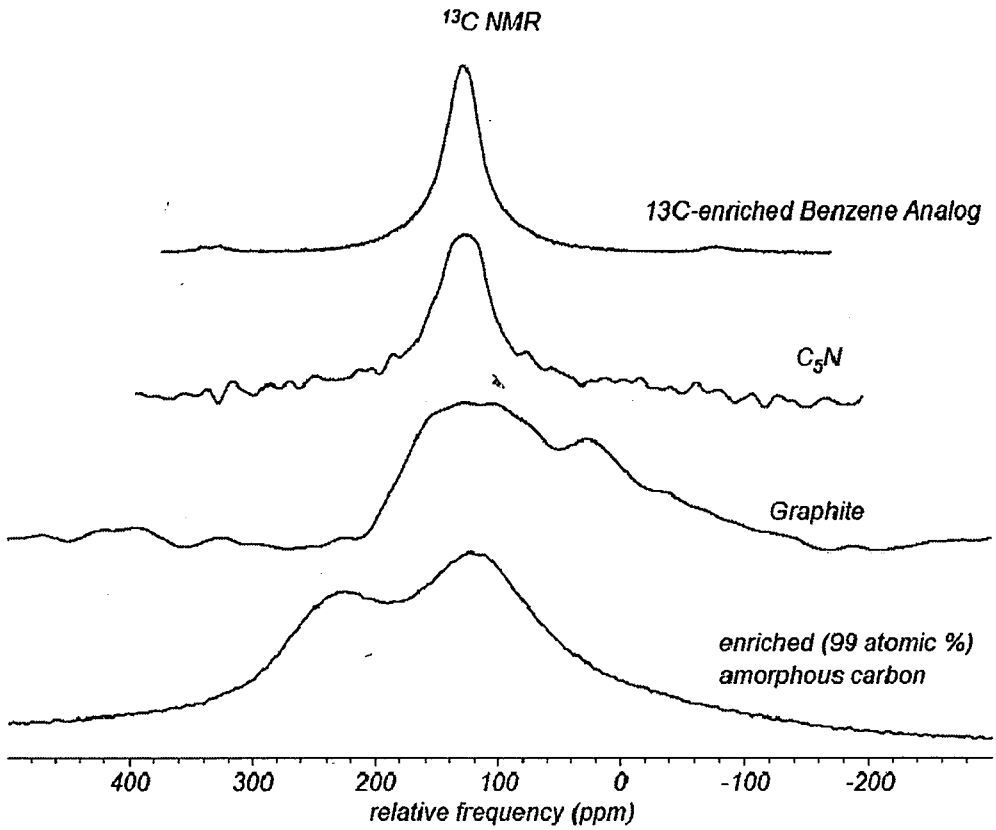

Figure 30 - ^{13}C-NMR Spectra of Various Carbons

It was surprising to find that C_5N and its benzene analog share a similar spectrum indicating aromatized sp^2 carbons. These spectra are remarkably simpler than would be expected. The signals overlap similar regions observed for graphite and amorphous carbon while the latter show additional complexity attributed to varying chemical domains. This supports the designation of the materials under study as graphite-like.

In order to obtain improved chemical information about the nature of the nitrogen in C_5N, a ^{15}N-enriched product was obtained from the enriched pyridine precursor and its ^{15}N-NMR spectrum was obtained as displayed in Figure 31.

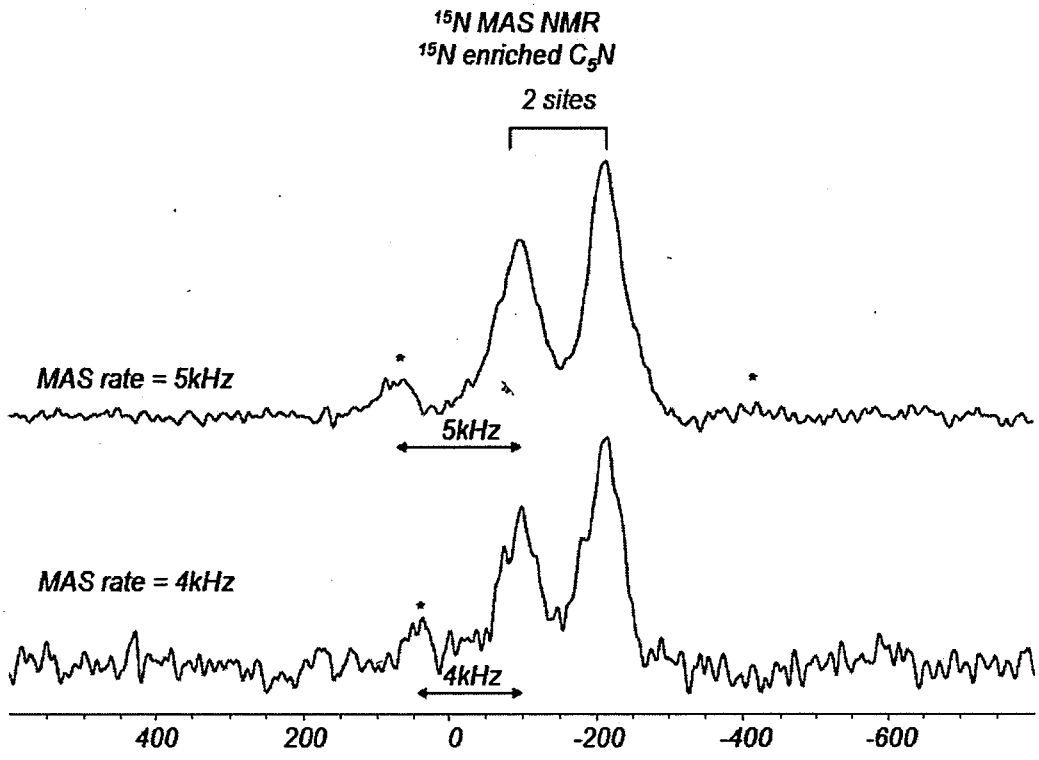

Figure 31 - ^{15}N-NMR of ^{15}N-enriched C_5N

Here there are two clear chemical environments at approximately -200ppm and -100ppm. The signal near -100ppm possesses a spinning side band at higher fields. This peak is assigned to sp^2-hybridized pyridyl nitrogen while that at -200ppm is consistent with aryl-bonded tertiary amine. The integral analysis of each of these indicates approximately 1:1 quantitative correlation. This is remarkably consistent with the XPS results and supports that the XPS analysis most likely represents the bulk material and is not just a partial sampling limited to a chemically unique surface. Again, this information supports the concept that the C_5N produced in this study possesses the correct structural bonding of a nitrogen-doped graphite-like material that is lacking order.

Finally, it was deemed important to evaluate the oxidation onset potential for C_5N in comparison with its benzene analog and graphite. This experiment can potentially say

something about the chemical environment in C_5N. Preparing each carbon substrate as an active electrode (see experimental section) enabled cyclic voltammetry to be performed on C_5N, its carbon analog, and graphite in a 1M solution of $LiPF_6$ in a mixture of ethylene carbonate and dimethyl carbonate. The oxidation onset potential as classically defined[92] for C_5N at 5.20 V (Li/Li+) was nearly 170 mV lower than that of its benzene analog and 620 mV less than graphite. This general trend is expected based on what is known about relative order and the effects due to nitrogen. C_5N also demonstrated semi-reversible behavior indicating the presence of some graphitic character, however the current for the reversible behavior decreased by nearly 10-fold for each potentiometric sweep cycle. The benzene analog did not display any reversible behavior while graphite displayed crisp reversible behavior, validating its robust properties that enable its commercial exploitation in battery electrodes. A summary of the comparative electrochemical data can be found in Table 2. These electrochemical relationships are difficult to summarize but do confirm that nitrogen doped carbons are more easily oxidized. Having a more highly ordered C_5N may enable more suitable reversibility allowing a more direct comparison with graphite. The non-reversible behavior of the benzene analog remains a curiosity.

Table 2 - Electrochemical Behavior of Carbon Substrates in LiPF6 solution.

Substrate	Oxidation Onset (V vs. Li/Li+)	Reversibility Per CV Cycle
C_5N	5.20	~10%
Benzene Analog	5.37	0%
Graphite	5.82	>95%

The culmination of the analytical evaluations described for C_5N in comparison with its benzene analog and graphite largely indicates that the material as formed in this study is highly

amorphous but possesses the appropriate bonding to be classified as a graphite-like carbon. Many of the studies described here confirm much of that reported by Bartlett and Labes in the 1980's. The major difference in the reports and observations in this study are mainly centered on the relative quantity of the two different types of nitrogen centers. This difference may be real, but may also be attributable to the application of more precise and advanced analytical instrumentation. By comparison with the benzene analog of C_5N and pristine graphite, it is concluded that the synthetic method and conditions are the determining factor in the acquisition of the poorly ordered products leaving way for future improvements in synthetic methodology. Some of these improvements may include but are not limited to the use of catalysts to enhance surface-specific growth, the application of hydrogen-deficient precursors such as cyanogens, and a high-pressure, high-temperature curing method such as the application of a multi-anvil press as suggested by Professor Landskron.

Intercalation/Reaction

One quite novel application of the current study is the attempt to oxidatively intercalate C_5N and its benzene analog, which is historically a quintessential test for graphitic character and oxidative chemistry. One of the most controllable and clean oxidants for intercalations of graphitic materials is peroxydisulfuryl difluoride, or $S_2O_6F_2$.

The utilized preparation of $S_2O_6F_2$ closely follows that developed by Bartlett, et al.[93] and is based on the reaction of xenon difluoride with fluorosulfuric acid and is described in greater detail in the Experimental section. One new observation in regards to its preparation and storage is that FEP™ appears to be unsuitable as the $S_2O_6F_2$ was found to swell the polymer and bleed through hydrolyzing on the exterior in contact with moist air. To solve this problem, CTFE polymer or alloy 400 vessels were used without additional problems.

The method of reaction of C_5N, its benzene analog, and graphite with $S_2O_6F_2$ was adapted from one of the experiments described by Biagioni[94] in which the solid carbon substrates were treated with the peroxide's vapor at room temperature until no further pressure drop was observed, over a number of hours. All three substrates adopted a blue-tint upon completion of the $S_2O_6F_2$ addition, indicating at least a minimum graphitic character; the graphite produced a deep blue material, C_5N was slightly blue, and the benzene analog only produced a blue hue when illuminated with a bright halogen or incandescent source. After thorough evacuation, the gravimetric uptake of $S_2O_6F_2$ was equated to an empirical formula of a fluorosulfate derivative as summarized in Table 3.

Table 3 - Gravimetric Uptake of $S_2O_6F_2$ on Carbon Substrates

Substrate	% wt Increase	Estimated Empirical Formula
C_5N	12	$C_{55}N_{11}$-OSO_2F (or $[C_5N]_{11}$-OSO_2F)
Benzene Analog	7	C_{120}-OSO_2F
Graphite	42	C_{20}-OSO_2F

This variable uptake of peroxide demonstrates the lack of order in the samples prepared by atmospheric reactive condensation. If the original investigators of C_5N attempted its intercalation with $S_2O_6F_2$, it is possible that it was never reported as a result of the poor success of the test; alternatively it may have been determined to be of little value since the characterization of amorphous materials is often inconclusive. Nonetheless, this is the first report the reaction of graphite-like C_5N and its benzene analog with $S_2O_6F_2$ and their analysis as covered in the following section.

Analysis of $S_2O_6F_2$ reacted material

The carbon materials treated with $S_2O_6F_2$ were analyzed by Raman confocal spectroscopy inside of FEP sample tubes. In general C_5N and its benzene analog do not show any shifts in frequency or relative intensity for the G and D-bands indicating little actual intercalation of graphitic domains but rather surface oxidation. These can be observed in Figures 32 and 33 respectively. The strong signals at 800cm^{-1} for fluorosulfate[86] are present in both species. The fluorosulfate signal in the C_5N is relatively stronger than that of the benzene analog which is consistent with the observations in the gravimetric uptake of $S_2O_6F_2$.

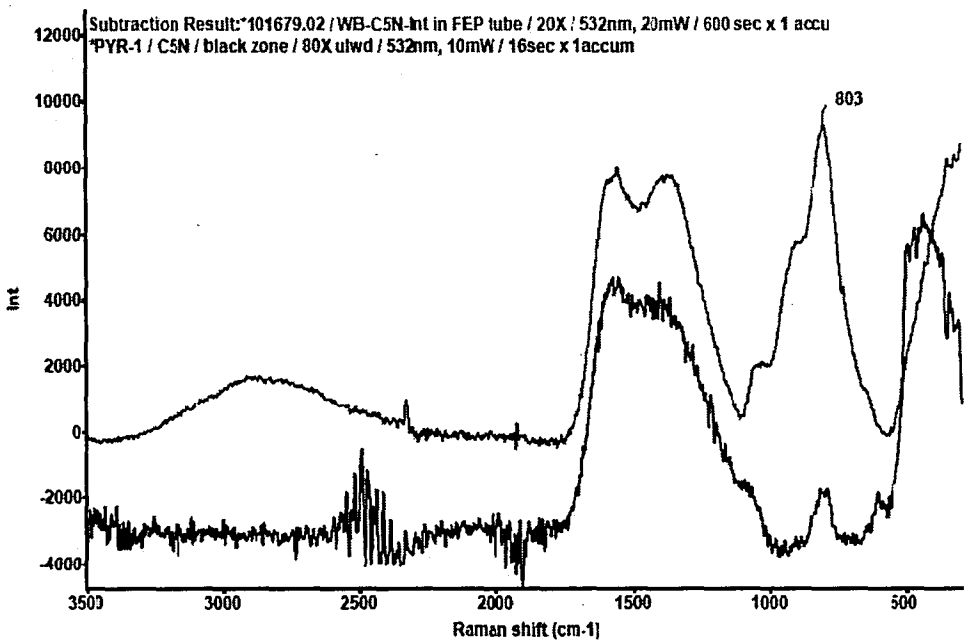

Figure 32 - Comparative Raman Spectra of C_5N (bottom) and C_5N Treated with $S_2O_6F_2$ (top)

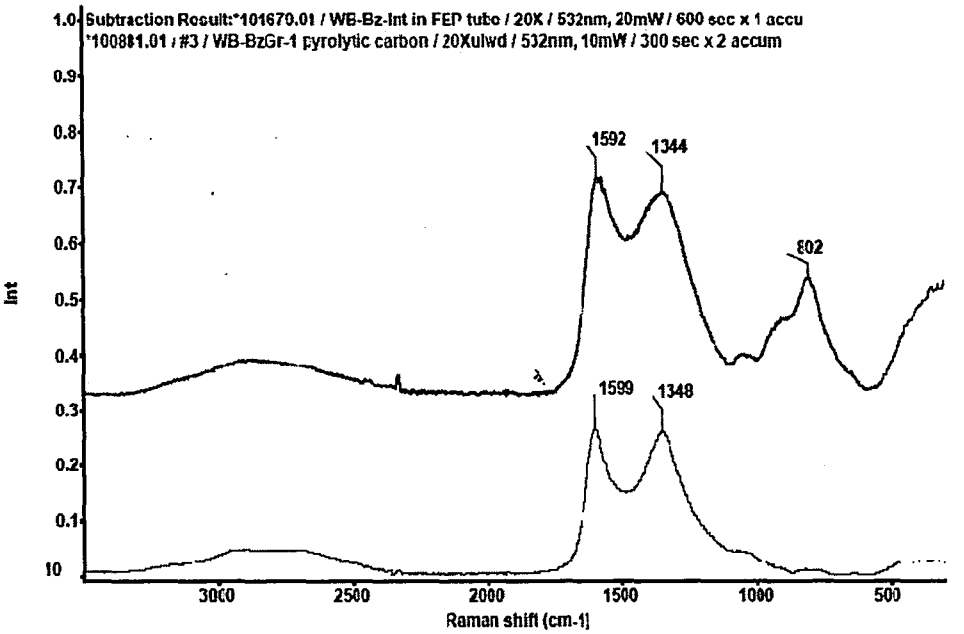

Figure 33 - Raman Spectra of The Benzene Analog (bottom) and That Treated with $S_2O_6F_2$ (top)

In stark contrast, graphite (Figure 34) shows a significant reduction in the G-band intensity and a shift in band frequencies indicating contracted bond order due to the oxidation of the graphite matrix. As expected, the intercalation markedly reduced the order of the system as apparent in the relative G/D band intensities. The fluorosulfate bands are also much larger than those from the C_5N and mirrors the gravimetric observations.

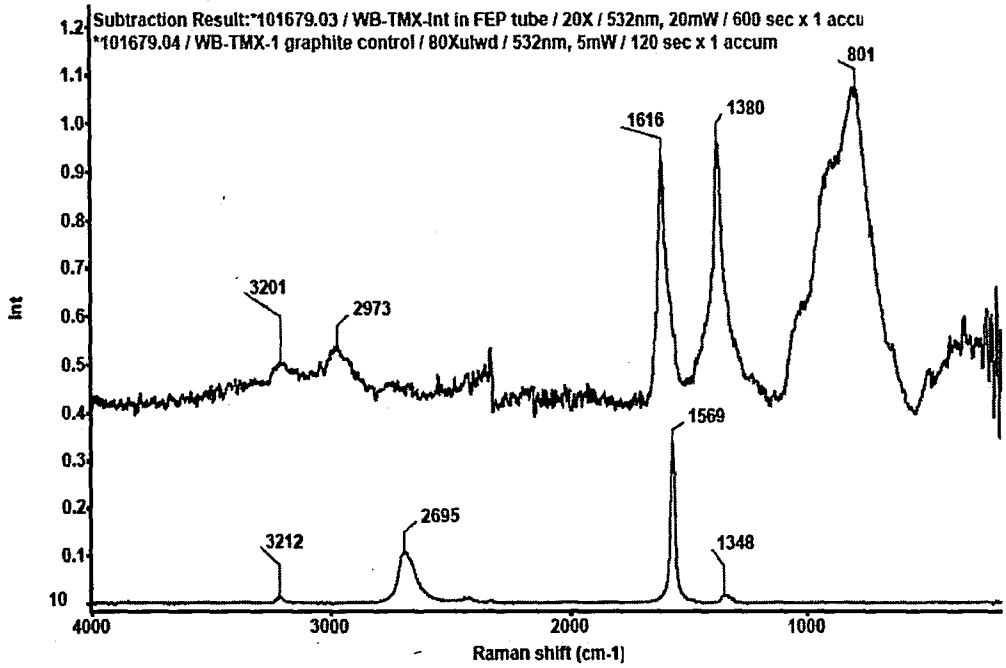

Figure 34 - Comparative Raman Spectra of Graphite (bottom) and Graphite Treated With $S_2O_6F_2$ (top)

The XRD analysis of the same carbons treated with $S_2O_6F_2$ indicate a significant loss of order to all carbons including the graphite shown in the overlaid spectra of Figure 35.

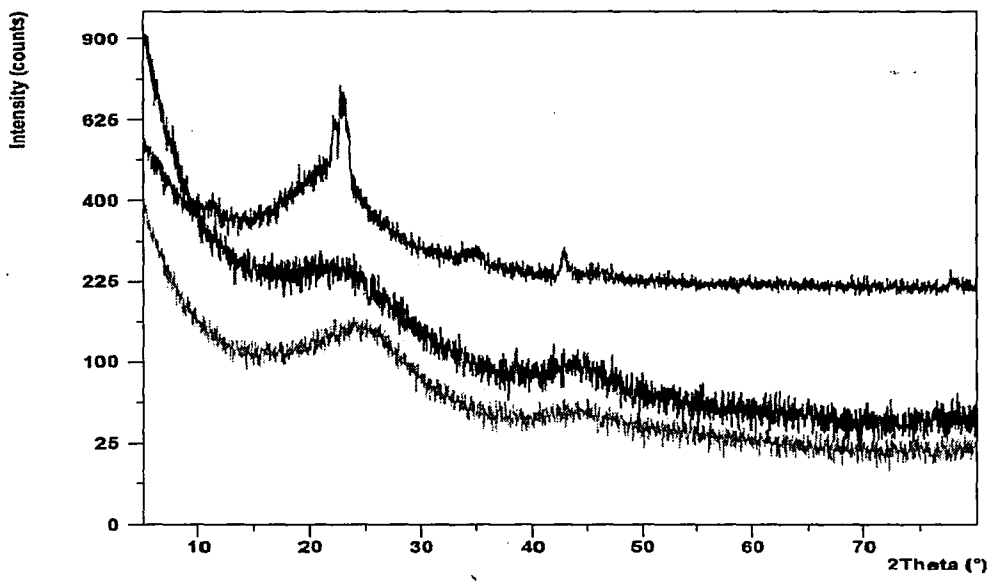

Figure 35 - XRD of C_5N (bottom), its Benzene Analog (middle) and Graphite (top) Treated With $S_2O_6F_2$

Here the peaks at 23-25° 2θ indicating the correct spacing for non-intercalated graphites have been somewhat diminished in intensity relative to the untreated materials indicating further loss of order upon reaction. Very small signals for graphite and the benzene analog can be observed at 11-12° 2θ indicating increased c-spacing to 7.6Å from 3.7Å and some ordered intercalated layers. The C_5N spectrum does not show such a peak. It is not unlikely for intercalated graphites to show diminished order parameters at intermediate or excessive levels of intercalation, however, shifts in the observed spacing does validate the presence of graphitic domains.

The XPS analysis of the $S_2O_6F_2$-treated carbons was also recorded in order to better understand the nature of the materials after oxidation with the peroxide. The C1s spectra of each (Figures 36-38) show the original binding energies for aromatic sp^2 carbons at 285 eV in the addition to a shoulder at 288 eV indicating carbons bound to the fluorosulfate intercalate. The quantitative analysis of these peaks relative to one another are consistent with the correct stoichiometry estimated by the gravimetric method described earlier with peroxide uptake decreasing on the order of Graphite>>C_5N>Benzene Analog.

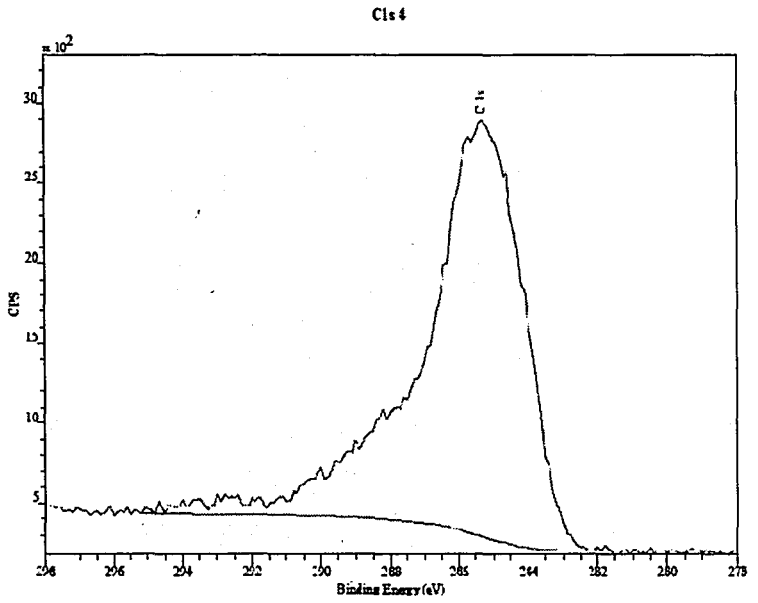

Figure 36 - C1s Spectrum of $S_2O_6F_2$ Treated C_5N

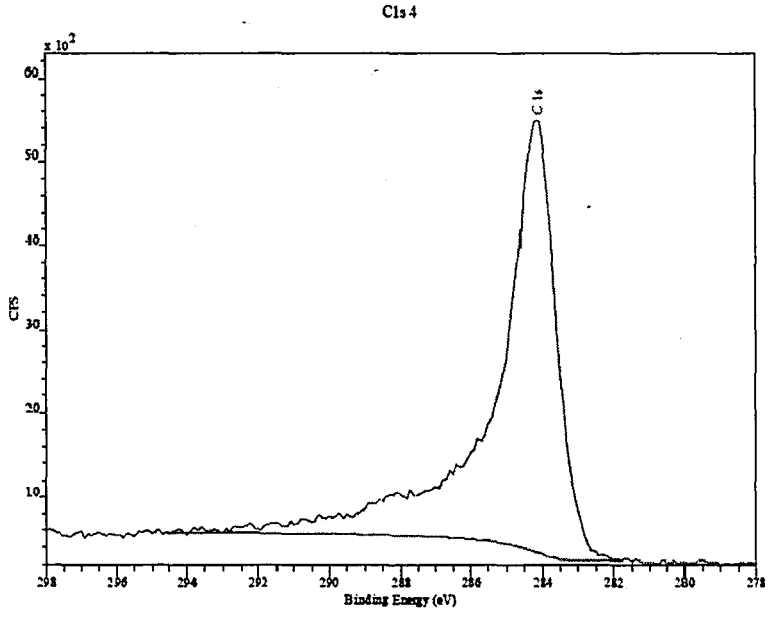

Figure 37 - C1s Spectrum of $S_2O_6F_2$ Treated Benzene Analog

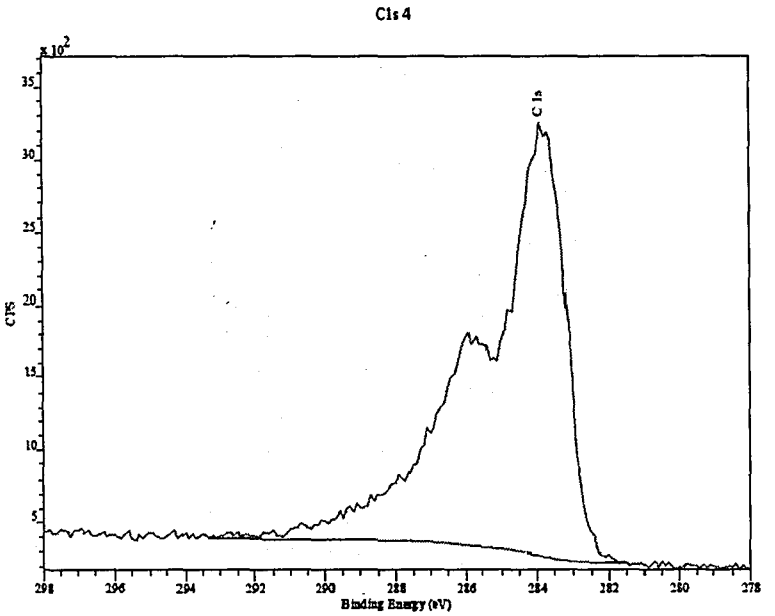

Figure 38 - C1s Spectrum of $S_2O_6F_2$ Treated Graphite

The N1s spectrum (Figure 39) of the treated C_5N does not vary much from that of the starting material indicating no apparent shift in charge from the nitrogen and no change in bond order as might have been expected from such a powerful oxidizer as $S_2O_6F_2$. However, the C1s spectra which do indicate shifts in bonding order and hybridization as a result of oxidative substitution.

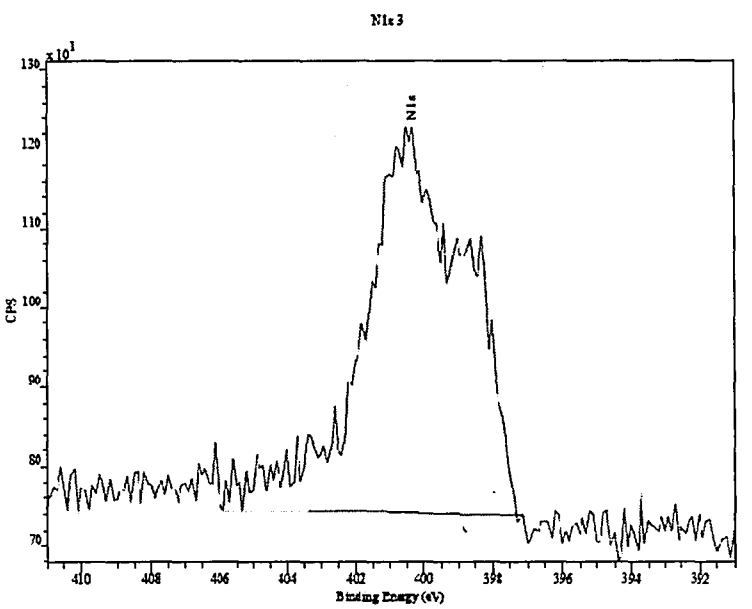

Figure 39 - N1s Spectrum of $S_2O_6F_2$-treated C_5N

The comparative ESCA analyses of each of the treated carbons indicates that no chlorine was lost in the course of the reaction and no nitrogen appears to have been lost from C_5N as it retains the appropriate C/N stoichiometry. The F, S, and O binding energies are consistent with those of fluorosulfate for each material at 686, 168, and 532 eV, respectively. The F/S/O/C ratios are all consistent with the estimates of gravimetric uptake with the exception that the oxygen in all samples are on the order of 2-3% mol higher than expected, possibly due to having already been in the starting material or due to some hydrolysis of the fluorosulfate anion by adventitious moisture. The CHN, S, Cl, and F elemental analysis of each material confirmed these results to within 2% mol deviation. The XPS analysis has confirmed the reactive substitution of $S_2O_6F_2$ onto each of the three carbon substrates, and does indicate a lack of order on the laboratory prepared materials as a result of their reduced uptake but still indicates a small amount which escalates expectations for future studies to produce higher ordered materials without loss of nitrogen.

In following the results of the XPS chemical environment analysis, solid-state NMR was performed in order to complement this understanding. The ^{19}F-NMR of the three materials (Figure 40) shows a relatively interesting phenomenon in regards to the fluorosulfate signals. There appears to be two different peaks; the most prominent peak in each of the materials is attributed to anionic fluorosulfate while a second signal at higher fields is indicative of carbon-bound fluorosulfate. In addition, some traces of HF at lower fields can be observed, possibly due to handling methods.

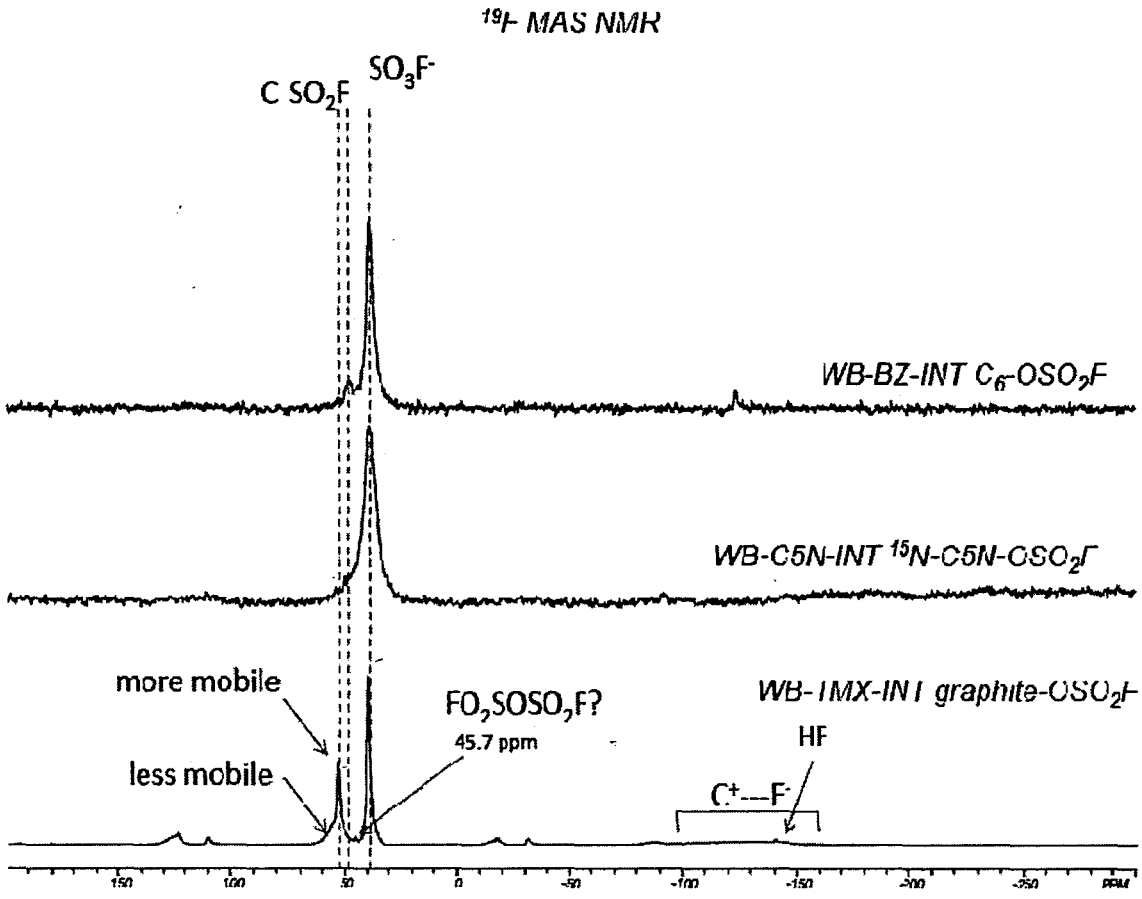

Figure 40 - ^{19}F NMR of $S_2O_6F_2$-Treated C_5N (center), Benzene Analog (top), and Graphite (bottom)

The ^{13}C NMR spectra for the treated materials are similarly displayed in Figure 41. Overlaid with their spectra prior to fluorination, one can see that little change is observed in absolute chemical shift within experimental uncertainty. The exception to this is in regards to the carbon spectrum of the intercalated graphite now showing an extremely sharp peak possibly due to the disruption of the systemic conductivity upon intercalation allowing a sharper spectrum to be obtained.

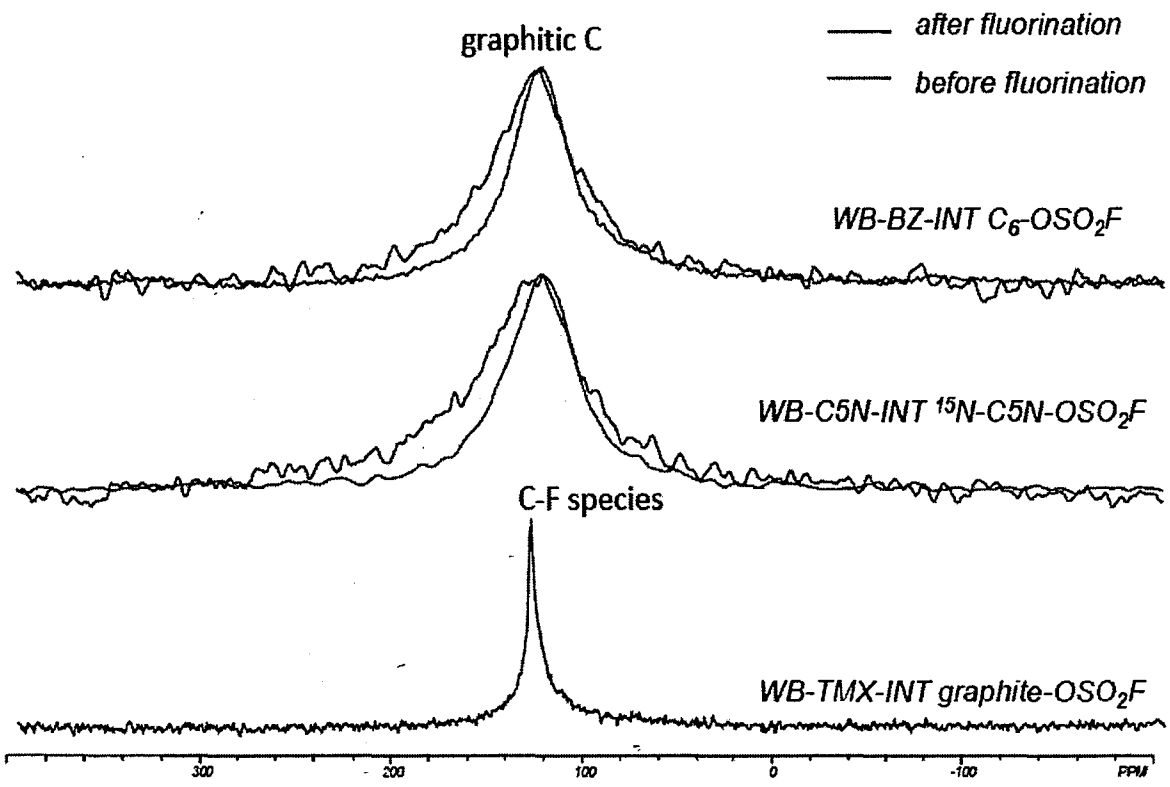

Figure 41 - ^{13}C NMR of $S_2O_6F_2$-Treated C_5N (center), Benzene Analog (top), and Graphite (bottom)

The signals due to nitrogen as seen in Figure 42 show no deviation from those of the starting materials. This is consistent with the observations made by XPS and further indicates that there is no definite change in electronic structure for the nitrogen regions of the C_5N after oxidative treatment.

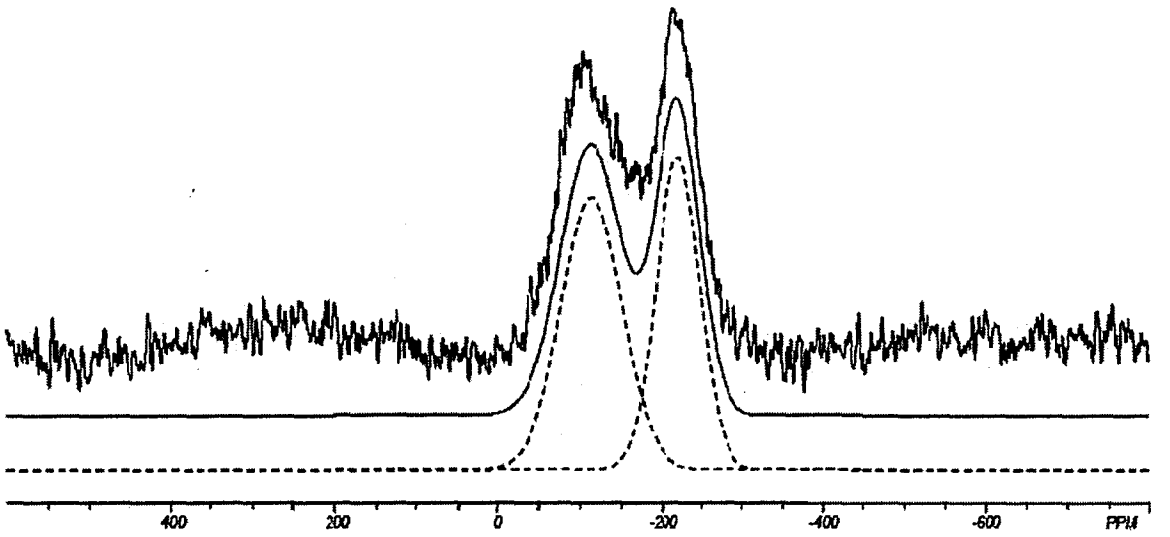

Figure 42 - ^{15}N NMR spectrum of $S_2O_6F_2$-Treated, ^{15}N-enriched C_5N

High resolution TEM of the treated materials (Figures 43-45) shows a significant reduction in order in comparison with the untreated precursors. The graphite image does show a measurable increase in the interlayer spacing which is consistent with intercalation theory but also displays considerable domains of relatively amorphous clustering. While some layering and extended networks could be observed in the C_5N and benzene analog precursors, none of these features could be found after treatment with $S_2O_6F_2$, making difficult the direct observation of microscopic intercalation mechanisms.

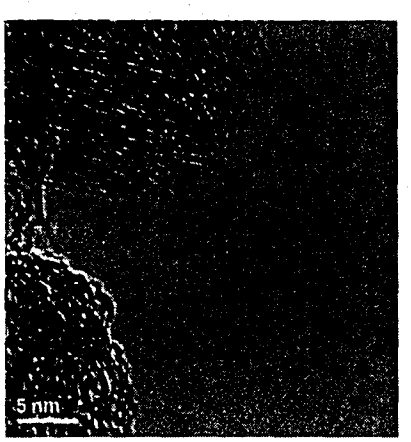

Figure 43 - HRTEM of $S_2O_6F_2$-Treated Graphite

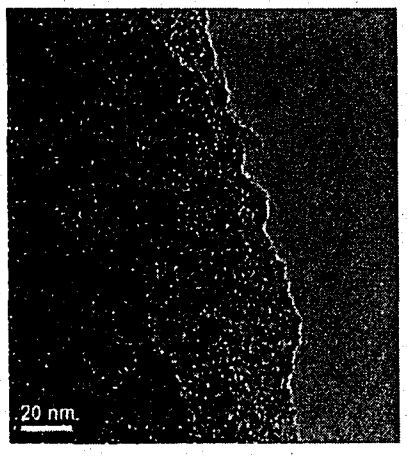

Figure 44 - HRTEM of $S_2O_6F_2$-Treated C_5N

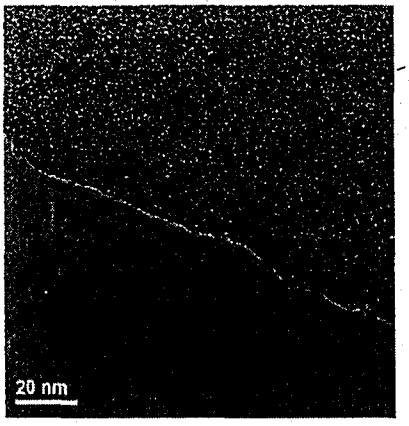

Figure 45 - HRTEM of $S_2O_6F_2$-Treated Benzene Analog

The EELS spectra collected from these images confirm the detracted order of each of the treated samples. As seen in the comparative examples of Figures 46-48, the broadness of the carbon edge signals generally indicate amorphous carbons which maintain a reasonable amount of sp^2 character as evident from the π to π^* position and intensity.

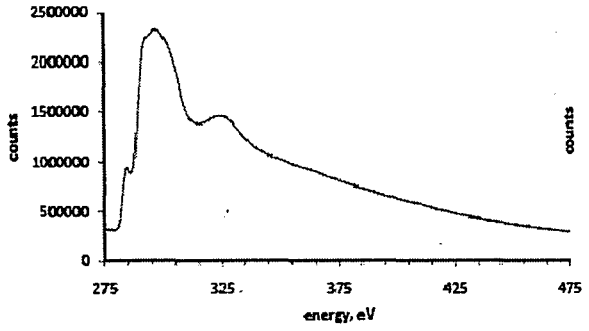

Figure 46 - EELS C-Spectrum of $S_2O_6F_2$-Treated Graphite

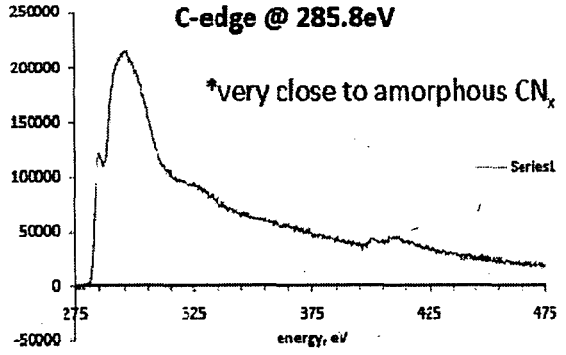

Figure 47 - EELS C-Spectrum of $S_2O_6F_2$-Treated C5N

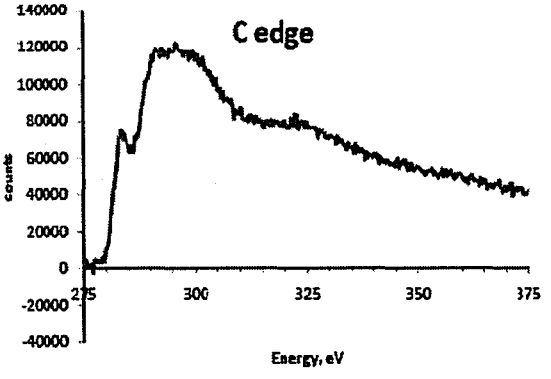

Figure 48 - EELS C-Spectrum of $S_2O_6F_2$-Treated Benzene Analog

The nitrogen-edge EELS of treated C_5N was also obtained and may be viewed in Figure 49. Here, the spectrum appears to be subdued in intensity and is attributed to signal dilution caused by the additional atoms represented by the fluorosulfate substituents. The spectrum has not changed, though, from its precursor, still showing measurable sp^2 character as evident from the π to π^* position and intensity.

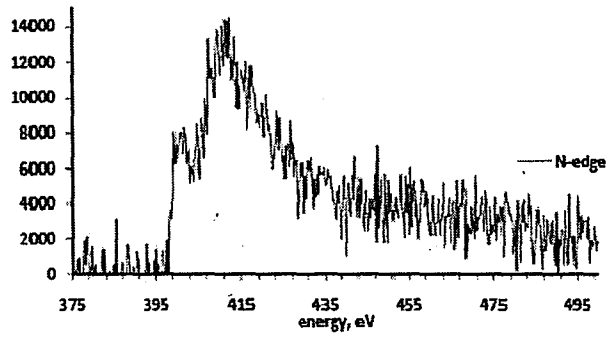

Figure 49 - EELS N-Spectrum of $S_2O_6F_2$-Treated C_5N

The EELS spectra in this case are confirming the loss of order and lack of an effect on the general chemical environment that reaction with S2O6F2 has on these carbon substrates.

Due to the prohibitive cost and time required for continued analysis, the pursuit of S, F, O, and Cl edge spectra were not ensued; these however, may prove interesting to study in future investigations in order to evaluate if and how they may affect the delocalized electrons of the graphite-like materials.

Summary

The nature of C_5N is based on poorly ordered sp^3 and sp^2 nitrogens bound in a matrix of sp^2 carbon. Hydrogen and chlorine contamination is also present in small quantities. As previously reported for C_5N, it is electrically conductive but somewhat less so than pure graphite. The diminished order is not due to random placement of or sheet deformation caused by nitrogen but appears to be primarily due to the synthetic process conditions as discerned from the analog produced by reacting of benzene with chlorine. XRD analysis does indicate trace evidence of sheet spacing similar to that of graphite but on a sparse and very small scale. This was confirmed by HRTEM observations of non-planar sheets overlapping in isolated domains. The presence of nitrogen does have an apparent effect of reducing the oxidation onset potential.

Attempts to "intercalate" C_5N have led to an interesting set of results. The reaction of all three carbon substrates led to materials that were poorer in order, possibly due to the disruption of inter-sheet order even on the smallest scale. The spectroscopic analysis of the products confirms the presence of fluorosulfate substituted carbon in all three substrates. This latter point does not confirm the presence of graphitic domains but does prove aromatic oxidation chemistry. It is interesting to point out that the nitrogen atoms did not adopt some positive charge upon reaction with $S_2O_6F_2$ as was originally hypothesized. This could be due to an effect of the tertiary amino nitrogen atoms activating the extended carbon rings toward oxidation substitution chemistry.

These points confirm the original designation of C_5N as "graphite-like". The need to better understand the utility and properties of a single phase of C_5N which is graphitic still exists. The thermal annealing of C_5N to a graphitic state is not directly possible due to the excessive loss of nitrogen. Dr. Landskron has suggested that annealing the C_5N at high temperature and pressure may be a more direct route to obtaining small quantities of highly ordered material to study and learn from. Future investigations may need to be centered around attempts to graphitize C_5N as it is known today in order to better characterized its beneficial properties as a highly ordered material rather than attempting numerous other methods of depositing a thermally and reductively sensitive material. Alternative synthetic methodologies would most likely be pursued upon finding evidence of promising and useful properties. Such syntheses should be designed to maximize deposition at the surface and incorporate substrates that do not induce hydrogen and chlorine contamination in the product. Without obtaining a more highly ordered C_5N, complex and expensive analytical methods such as neutron diffraction-paired distribution function analyses would be required.

Experimental

Safety

A number of the reactants and byproducts employed in the synthetic schemes in this study are potentially hazardous and/or toxic. Chlorine, xenon difluoride, benzene, pyridine, hydrogen fluoride, peroxy disulfuryl difluoride, cyanogen, cyanogen fluoride, and hydrogen cyanide each represent materials that are either highly reactive, highly toxic, or both and should be researched thoroughly and hazards considered carefully before using or making them. Of particular concern is the potential for HF exposure, which has the unique ability of inducing fluoride intoxication even with small exposures to any surface of the body. Calcium gluconate antidote should be considered as an anti-active in the chance that an HF exposure is obtained.

High temperatures are employed in various steps of experimental procedures and may present potential for burns. High temperature surfaces and heating elements may also provide active surfaces that can initiate violent reactions or ignition of flammable materials.

Glassware and quartz are used under extreme conditions and slight pressures giving the possibility for fracturing and exposure to sharp pieces. Glassware should be carefully inspected for defects and cleaned thoroughly before and each use.

Gases under high pressure are also employed in this study. Careful consideration and designs should be exercised in their deployment to ensure that no other system components can be over-pressurized or expose the operator to any toxic gases.

Analytical Tools

Numerous analytical instruments were employed in the analylsis of C_5N, its benzene analog, graphite, and their respective $S_2O_6F_2$ treated adducts. Listed here are the instruments and services employed:

The XPS experiments were carried out on a PHI 5000VersaProbe XPS spectrometer, which is equipped with multi-channel plate detectors (MCD) and an Al monochromatic X-ray source. The XPS data were collected using Al X-ray excitation (50W and 15 kV). The low-resolution survey spectra were collected at 117.4 eV pass energy, 50 msec dwell time, and 1.0 eV/step. The high-resolution regional spectra were collected at 23.5 eV pass energy, 100 msec dwell time, 0.1 eV/step. The profile data were collected at 58.7 eV pass energy, 100 msec dwell time and 0.150 eV per step. The analysis area is 200 □m and a take-off-angle of 45□. The quantitative elemental analyses were determined by measuring the peak areas from the high-resolution regional spectra and applying the transmission-function corrected atomic sensitivity factors. The PHI SUMMITT software was used for data collection and the CASA software was used for data analysis. Where applicable, the etch rate is calibrated against 20.3 nm SiO2/Si from Sigma Optical Metrology Consulting. The ion gun settings are 5 kV, 2 uA, 4mm x 4mm raster. XPS samples were loaded on conductive silicon adhesive tape to the analysis puck in an argon-purged glove box and transferred into the instrument in a sealed inert transfer vessel ensuring that the samples do not become exposed to atmospheric moisture.

High resolution STEM and EELS spectra were obtained with the JEOL 2010FasTEM located at the University of Delaware (W.M. Keck Microscopy Center). This is a transmission electron microscope equipped with a Schottky field emission source typically operated at 200keV. Point to point imaging resolution in TEM mode is 1.9 Å and lattice imaging resolution is

1 Å. Imaging in STEM mode provides a lattice resolution of 1.9 Å. The JEOL 2010FasTEM is also equipped with a GATAN imaging filter (GIF) that allows for energy filtered imaging and electron energy loss spectroscopy (EELS) in both TEM and STEM modes. EELS spectra can be captured with a typical energy resolution of 1.5 eV and a spatial resolution down to 2 Å in STEM mode (dependent on sample). The JEOL 2010FasTEM is also equipped with an EDAX energy dispersive X-ray spectrometer that can be operated in either TEM or STEM mode with an energy resolution of 132 eV.

X-ray diffraction was performed using a Panalytical X'Pert PRO MRD with a Cu X-ray tube, an X-ray mirror equipped with an automatic 0.2mm Cu/Ni beam attenuator and ½° divergence slit on the incident beam, a parallel-plate collimator with 0.09° of collimation on the diffracted beam, and a proportional gas-ionization detector with a detection efficiency of 84% and a linear range up to 10^6 cps. Samples were mounted as sealed capillaries on a horizontally mounted, high resolution goniometer with a minimum step size of 0.0001°. Diffraction patterns were collected over a range of $10° \leq 2°\theta \leq 85°$.

The ^{13}C-NMR static echo experiments for natural and synthetic graphites were performed with an echo time of 2 ms and pulse delay of 20 s at the Bruker™ DMX-500 FT-NMR spectrometer equipped with a Doty XC5 probe. The ^{13}C static echo experiment with 2 ms of echo time and ^{15}N MAS NMR experiment with spinning speed of 5 kHz for ^{15}N-enriched C_5N sample were performed at Bruker Avance™ II-300 FT-NMR spectrometer equipped with a BL7-VTN probe with pulse delays of 60 s. The pulse delays for ^{13}C, ^{15}N and ^{19}F MAS are 5-30 s, 20 s and 1-5 s, respectively. The chemical shifts of ^{1}H, ^{13}C and ^{19}F were referenced to TMS, TMS, and $CFCl_3$, respectively. The chemical shifts of ^{15}N were referenced to CH_3NO_2 using a secondary standard $^{15}NH_4{}^{15}NO_3$ (-358 ppm for NH_4 peak). All samples were packed into a 3.2mm zirconia rotor with a Kapton™ sealing cap.

Raman spectra were obtained with a Kaiser Holoprobe™ Raman spectrometer coupled to an Olympus BX 60 microscope under the following operating with a 532 nm laser at 5 mW power. The microscope was equipped with a 20x ultra-long working distance objective and the spectral path was composed of multimode optical fibers. All samples were collected using a 90 second integration time.

FTIR analysis was afforded using a Thermo Nicolet Smart Orbit™ ATR accessory and diamond ATR crystal. A portion of the sample was pressed onto the crystal and a spectrum obtained by co-adding 128 scans at 4.0 cm^{-1} resolution using a Nicolet Nexus™ 750 FT-IR interferometer.

Gas phase FTIR analysis of the pyrolytic CVD reactor's effluent was performed using a MIDAC M-Series FTIR fitted with KBr optics. The gas cell employed was fabricated from Nickel-200 alloy to resist corrosion, possessed a pathlength of 10cm, and was terminated with paired 25x2mm ZnSe and AgCl windows with the AgCl facing the internal portion of the cell. The spectrometer was controlled and spectra were collected and analyzed using the EssentialFTIR™ software package.

Scanning electron microscopy (SEM) was performed on ground samples of carbons by mounting directly on double-stick carbon tape on aluminum SEM sample stubs. No conductive coating was applied to the specimens. Scanning electron microscopy (SEM) observation was performed using a Hitachi S-4800 field-emission SEM. Images were obtained at X100, X1000, X5000, X20,000, and X50,000 magnification using the upper secondary electron detector, mixing in 50% low angle backscattered electrons. All images were obtained using an accelerating voltage of 2 kV with 10 microamps of beam current. Energy-dispersive x-ray microanalysis (EDS) was performed in the Hitachi S-4800 using a Thermo Noran™ System Six EDS system. EDS

spectra of typical areas were acquired at 10 kV accelerating voltage in high beam current mode using the Noran Point & Shoot method using a spectrum acquisition time of approximately 40 seconds per point or area.

CHN and chlorine analysis was performed by Schwarzkopf Microanalytical Laboratories located in Woodside, NY. The methods used incorporated combustion followed by secondary analysis by gas or ion chromatography.

Deposition Reactions

The atmospheric vapor deposition reactor is a simple flow reaction system for combining two reactants in a heated zone. For reference to the description, refer to Figure 50.

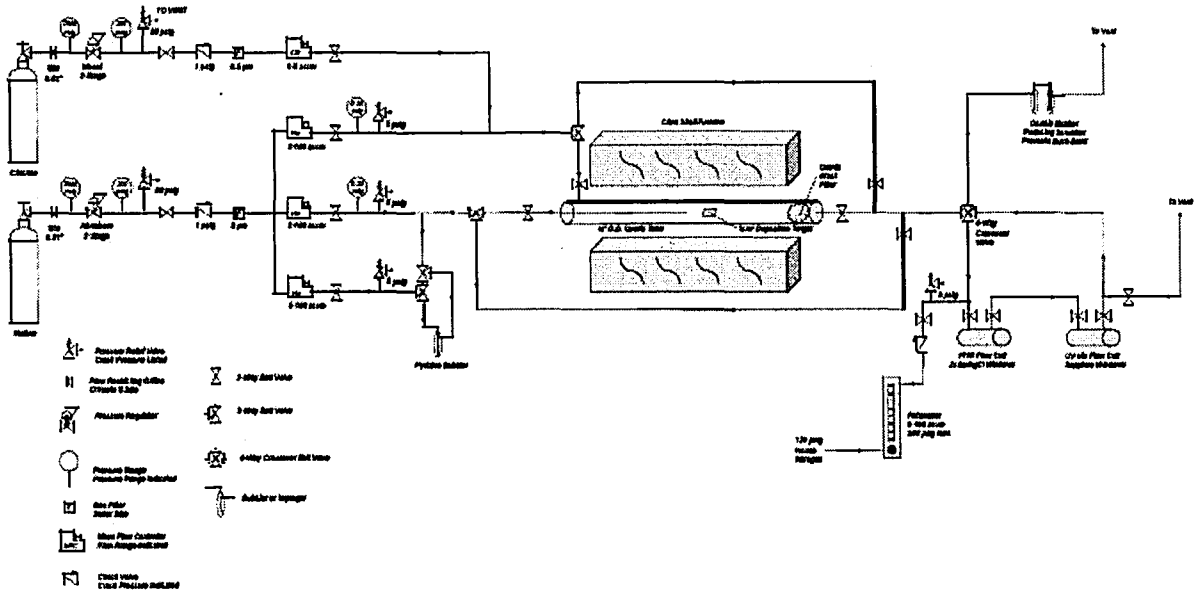

Figure 50 - Reaction Flow System For C_5N Synthesis

The chlorine diluent gas (either N_2 or He) is fed into the front end of the process by Brooks mass flow controllers (model 5850). The chlorine is directly blended down with the

diluent gas and passed into the reactor's outer sheath or can be diverted around the reactor to a scrubber. The second reactant stream is produced by bubbling diluent gas[95] through a hydrocarbon precursor, which is presumed to saturate the gas at a particular temperature to enable a specified vapor concentration to be produced. This stream can be diluted further by blending with additional diluent gas, eliminating the need for strict temperature control over the hydrocarbon which may have the tendency of freezing at the temperatures needed to obtain relatively low vapor concentrations. The hydrocarbon stream can be diverted around the deposition reactor if needed or passed directly to the heated zone of the reactor through an inner quartz tube because some hydrocarbons (i.e. pyridine) may react with chlorine to produce non-volatile products before even entering the heated reactor.

The reactor was comprised of a quartz tube with inner tube. The outer quartz tube was either 19 or 30mm in diameter, both with a length of 18 inches. This length is somewhat shorter than conventional furnace tubes because it was desirable that these could be placed into a glove box ante-chamber. The position of the inner tube of ¼" outside diameter could be varied to affect yield and positional delivery of the hydrocarbon precursor. Quartz or sapphire plates, if desired, could be placed in the reactor in order to collect deposits at any position throughout the reactor. The exit of the reactor was stuffed with quartz-fiber wool to trap any fine particulates or condensing matter that may fowl the down-stream lines. From the exit of the reactor, the stream of gas could be diverted through FT-IR (10cm Alloy 200 cell with AgCl and ZnSe windows) and UV-Vis spectroscopy (5cm glass cell with sapphire windows) cells to analyze for product gases including HCl, HCN, ClCN, NCCN, precursors, and chlorine (UV-Vis). All gases exit the system by first bubbling through a 60mL caustic sulfite scrubber (10% Na_2SO_3 and 20% NaOH) then passing into the hood ventilation system.

The vulnerable components of the system were protected against over-pressurization by placement of pressure relief valves (500 series Circle Seal valves set to 3 psid cracking pressure) near each of the pressurized gas inlet sources. Gauges were also installed nearby these locations to aid in diagnosing any system flow problems or component malfunctions.

The quartz tubes were inserted into a horizontal tube furnace. The 19mm tube was matched with a ¾" X 6" single zone furnace[96] while the 30mm tubes were used with a 1.5" X 12" single zone furnace, both of which were temperature regulated using fuzzy-logic control with over-temperature protection for safety.

By calculation, the concentration of hydrocarbon in diluents gas could be estimated as a function of temperature. Independent of the gas composition, the concentration of hydrocarbon was determined as a function of its vapor pressure relative to the absolute pressure (atmospheric pressure, or approximately 760 torr) of the carrier gas at the given temperature. The vapor pressure of pyridine[97] and benzene[98] were calculated based on literature-based Antoine relationships. A spreadsheet program was developed to accurately estimate vapor concentration of volatile liquids in gases by assuming vapor saturation and correcting for temperature dependent vapor density relationships[99]. Key temperatures that are easy to obtain and maintain were used in the approximation to determine the correct flow of carrier gas and additional diluent. Flow rate of carrier gas could then be converted into mass and molar flow of reactant and the correct addition of chlorine can then be dialed in. These calculations for specific temperature regions of pyridine and benzene are shown in Tables 4 and 5.

Table 4 - Pyridine vapor conveyance calculations

Temp. (C)	VP (mm Hg)	VP (atm)	Conc (mol/ml) @ STP	Conc (g/mL) @ STP	Pyr flow (g/hr) at 20 sccm gas	Pyr flow (sccm) at 20sccm gas	Cl2 Flow Needed for 2.5 eq (mL/min)
-2	3.723	0.00490	2.04E-07	1.61E-05	1.93E-02	9.12E-02	2.28E-01
-1	3.998	0.00526	2.19E-07	1.73E-05	2.08E-02	9.80E-02	2.45E-01
0	4.290	0.00564	2.35E-07	1.86E-05	2.23E-02	1.05E-01	2.63E-01
1	4.600	0.00605	2.52E-07	1.99E-05	2.39E-02	1.13E-01	2.82E-01
2	4.930	0.00649	2.70E-07	2.13E-05	2.56E-02	1.21E-01	3.02E-01
19	14.542	0.01913	7.95E-07	6.29E-05	7.55E-02	3.56E-01	8.91E-01
20	15.418	0.02029	8.43E-07	6.67E-05	8.01E-02	3.78E-01	9.45E-01
21	16.339	0.02150	8.94E-07	7.07E-05	8.48E-02	4.00E-01	1.00E+00
22	17.306	0.02277	9.47E-07	7.49E-05	8.99E-02	4.24E-01	1.06E+00
23	18.322	0.02411	1.00E-06	7.93E-05	9.51E-02	4.49E-01	1.12E+00
24	19.387	0.02551	1.06E-06	8.39E-05	1.01E-01	4.75E-01	1.19E+00
25	20.504	0.02698	1.12E-06	8.87E-05	1.06E-01	5.02E-01	1.26E+00
26	21.674	0.02852	1.19E-06	9.38E-05	1.13E-01	5.31E-01	1.33E+00
27	22.901	0.03013	1.25E-06	9.91E-05	1.19E-01	5.61E-01	1.40E+00
40	44.968	0.05917	2.46E-06	1.95E-04	2.33E-01	1.10E+00	2.75E+00
60	111.585	0.14682	6.10E-06	4.83E-04	5.79E-01	2.73E+00	6.84E+00
80	243.731	0.32070	1.33E-05	1.05E-03	1.27E+00	5.97E+00	1.49E+01
100	480.525	0.63227	2.63E-05	2.08E-03	2.49E+00	1.18E+01	2.94E+01
115.2	760.569	1.00075	4.16E-05	3.29E-03	3.95E+00	1.86E+01	4.66E+01

Table 5 - Benzene vapor conveyance calculations

Temp. (C)	VP (mm Hg)	VP (atm)	Conc (mol/ml) @ STP	Conc (g/mL) @ STP	Bz flow (g/hr) at 20 sccm gas	Bz flow (sccm) at 20sccm gas	Cl2 Flow Needed for 3 eq (mL/min)
-2	20.886	0.02748	1.14E-06	8.92E-05	1.07E-01	5.12E-01	1.54E+00
-1	22.484	0.02958	1.23E-06	9.61E-05	1.15E-01	5.51E-01	1.65E+00
0	24.190	0.03183	1.32E-06	1.03E-04	1.24E-01	5.93E-01	1.78E+00
1	26.009	0.03422	1.42E-06	1.11E-04	1.33E-01	6.37E-01	1.91E+00
2	27.949	0.03678	1.53E-06	1.19E-04	1.43E-01	6.85E-01	2.05E+00
18	68.251	0.08980	3.73E-06	2.92E-04	3.50E-01	1.67E+00	5.02E+00
19	71.657	0.09429	3.92E-06	3.06E-04	3.67E-01	1.76E+00	5.27E+00
20	75.203	0.09895	4.11E-06	3.21E-04	3.86E-01	1.84E+00	5.53E+00
21	78.892	0.10381	4.32E-06	3.37E-04	4.04E-01	1.93E+00	5.80E+00
22	82.730	0.10886	4.53E-06	3.53E-04	4.24E-01	2.03E+00	6.08E+00
23	86.721	0.11411	4.74E-06	3.71E-04	4.45E-01	2.13E+00	6.38E+00
24	90.869	0.11957	4.97E-06	3.88E-04	4.66E-01	2.23E+00	6.68E+00
25	95.180	0.12524	5.21E-06	4.07E-04	4.88E-01	2.33E+00	7.00E+00
26	99.658	0.13113	5.45E-06	4.26E-04	5.11E-01	2.44E+00	7.33E+00
27	104.307	0.13725	5.71E-06	4.46E-04	5.35E-01	2.56E+00	7.67E+00
40	182.785	0.24051	1.00E-05	7.81E-04	9.37E-01	4.48E+00	1.34E+01
50	271.286	0.35696	1.48E-05	1.16E-03	1.39E+00	6.65E+00	1.99E+01
60	391.472	0.51509	2.14E-05	1.67E-03	2.01E+00	9.59E+00	2.88E+01
70	550.832	0.72478	3.01E-05	2.35E-03	2.82E+00	1.35E+01	4.05E+01
80	757.662	0.99692	4.14E-05	3.24E-03	3.88E+00	1.86E+01	5.57E+01
81	781.298	1.02802	4.27E-05	3.34E-03	4.01E+00	1.91E+01	5.74E+01

In a typical reaction, the reactor tube was assembled and purged with inert gas for at least 24 hours. Prior to a deposition experiment, the furnace was heated to the desired

temperature and maintained for at least 1 hour. In all cases, the hydrocarbon component was introduced first into the reactor followed by flow of the chlorine. At the completion of a synthetic run, chlorine flow was first stopped followed by the hydrocarbon. The reactor was then purged at the reaction temperature for 1 hour before returning to room temperature.

Product was isolated from the quartz tube by scraping from the surface with a long stainless steel spatula or directly extracting the sample plates with long forceps. All products were ground with a clean agate mortar and pestle while yields were calculated as mass of isolated product referenced to the stoichiometric ideal quantity of product based on the limiting reagent.

Preparation of C_5N by alternative substrates

Some alternative test precursors for the synthesis of C_5N including 3-cyanopyridine, 2,6-dicyanopyridine, 3-chloropyridine, and 2,6-dichloropyrdine were used in the deposition reactor without co-adding chlorine. Each of these materials does not have a sufficient vapor pressure for transport into the reactor alone. Their introduction into the heated zone of the reactor was accomplished by dissolution in anhydrous acetonitrile[100] to produce a 20%wt solution which was passed through a quartz nebulizer[101] that replaced the inner tube of the deposition reactor and extended well into the heat zone. The nebulizer was fed with the liquid precursor solution at a rate of 1ml per hour using a metering syringe pump. The support and spray gas was comprised of 60 sccm of helium.

All reaction cases produced extremely poor yields of C_5N under a reactor temperature of 700°C giving less than 5% of the theoretical yield based on available nitrogen and carbon not including that of the solvent. Barely enough product was isolated from each reaction to verify

the C_5N stoichiometry and demonstrate no detectable chlorine except in the case utilizing the dichloropyridine precursor where 0.06 mol% chlorine was found.

Electrochemical Setup

In order to evaluate the electrochemical performance of the carbons under study, they first must be made into an electrode that can be attached to the leads of a potentiometer as they are not soluble in any known solvent. First, 50 mg of the ground carbons were weighed into separate 30mL polypropylene round-bottomed centrifuge tubes with 8% relative weight (4 mg) polyvinylidene difluoride, 1 mL of N-methylpyrrolidinone, and three 10mm diatmeter ceramic bearings. To reduce the carbon particle size and homogenize the suspension, the tube contents were milled by rotating the tubes at a 45° angle at 0.5 revolutions per second over 48 hours.

The conductive substrate for the carbons consisted of platinum gauze[102] of 100 mesh cut into 5mm by 50mm strips. 1 cm of the platinum gauze tip was immersed into the carbon slurry and allowed to dry in a 60°C oven for 24 hours to allow hardening. This coating process was performed a total of three times to build up a sufficient amount of substrate for evaluation. The electrodes were then fully dried in a 120°C vacuum for 48 hours then stored in an argon-purged glove box for use.

Cyclic voltammetry experiments were conducted using a three electrode cell inside of an argon purged glove box. Alligator lead clamps were attached directly to the untreated end of the platinum gauze, forming the working electrode. A bare platinum coil wire electrode[103] comprised the counter electrode and pure lithium metal foil was used as a pseudo-reference. The electrodes were assembled into a 30mL cell using commercially available components[104,105].

The electrochemical cell was filled with 10mL of an electrolyte solution as previously described in the literature[106]. This solution was composed of 1M $LiPF_6$[107] in a 3:7 by weight mixture of ethylene carbonate[108] and dimethyl carbonate[109], respectively. The electrodes were placed in the solution and allowed to equilibrate for 10 minutes to ensure wetting of all surfaces.

A potentiostat (CHI model 660A) was used to measure the open circuit potential (OCV) of the cell to ensure proper connection of all electrodes. The same potentiostat was then used to perform cyclic voltammetry in multiple forward and reverse segments ranging from 3.0V to 6.0V versus Li/Li^+ at a scan rate of 0.01 mV per second. The voltammograms were then analyzed to determine the oxidation potential onset as evident by a sharp deflection in the differential in the lower potentials of the curve.

Synthesis of Peroxy-disulfuryldifluoride ($S_2O_6F_2$)

The $S_2O_6F_2$ used to react with the carbon test substrates was synthesized using a modified method described by Bartlett[110] as recounted here. A ½" fluorinated ethylene propylene (or FEP™,[111]) reactor tube[112] was fabricated by heat-sealing one end in a vise and forming a connection on the other using a Swagelok™ reducing fitting[113]. A second similar reactor was attached to the first using a length of 1/8" FEP tubing divided using a PFA plug valve[114]. The 1/8" tubing was fed into each reactor via a bored-through tee connection[115] enabling a valve[116] to access each reactor. In a nitrogen-purged glove box, xenon difluoride[117] (8.546 g, 0.0505 mol) was added to one tube and triple-distilled fluorine sulfonic acid[118] (10.100 g, 0.101 mol) was added to the other with the dividing valve closed. The sealed reactors were removed from the glove box and attached to a Monel™ vacuum manifold. The vessel containing XeF_2 was cooled in liquid nitrogen and the one with the FSO_3H was cooled in

powdered dry ice. The XeF_2 tube was evacuated to less than 10^{-3} torr then the Teflon valve dividing the two vessels was opened allowing the cold FSO_3H to flow in under the nitrogen pressure of the gas remaining from the loading process. Under these conditions, the FSO_3H solidified immediately upon contact with the wall of the vessel containing the XeF_2. The reactor was evacuated again and the remaining FSO_3H was allowed to slowly distill away from the walls of the vessel under its own vapor pressure to quantitatively condense over to the XeF_2.

The Teflon valve was closed and the mixture was allowed to warm to -78°C in powdered dry ice where the mixture slowly turned to a homogeneous yellow liquid. After standing for 4 hours, the mixture was allowed to warm to 0°C in an ice-water bath where, according to the literature, the complete conversion of XeF_2 is obtained. After 2 hours at 0°C the deeply yellow reactor contents were cooled back to -78°C. At this stage, the effective stoichiometric balance is represented by the equation:

$XeF_2 + 2\ FSO_3H \rightarrow Xe(SO_3F)_2 + 2\ HF.$

HF and traces of Xe gas were removed at -78°C under vacuum leaving behind the unstable xenon bis(fluorosulfate). Warming this material slowly to room temperature and allowing to stand for 48 hours decomposes the fluorosulfate complex to liberate Xe gas to produce high purity peroxydisulfuryl difluoride, or $(FSO_3)_2$ as represented in the equation:

$Xe(SO_3F)_2 \rightarrow Xe_g + S_2O_6F_2.$

The reactor was cooled once again to -78 to affect easy removal of xenon gas under vacuum and the reactor was sealed to contain the highly reactive peroxide until need for intercalation chemistry.

The gas phase infrared spectra obtained at 8 torr in a nickel 10cm cell fitted with ZnSe windows. Two spectra from duplicate samples are overlaid in Figure 51 showing the absence of

FSO_3H, HF, and $S_2O_5F_2$ rather only the strong vibrational modes of $S_2O_6F_2$ reported in the literature[119].

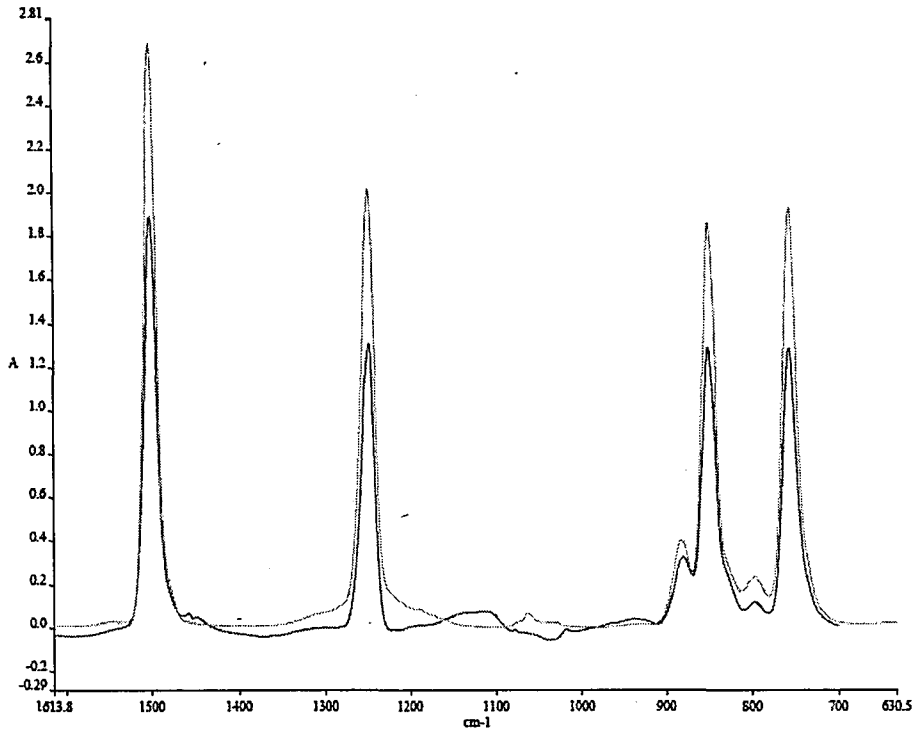

Figure 51 - Gas-phase FTIR spectrum of $S_2O_6F_2$

Reaction of Carbons with $S_2O_6F_2$

The carbons used in this study were dried by grinding in an agate mortar and pestle and heating to 400°C under a 20sccm flow of helium in a 1.5" quartz flow reactor. 150mg each of C_5N, ^{15}N-enriched C_5N, the benzene analog of C_5N, the ^{13}C-enriched benzene analog of C_5N, and graphite were loaded to 3/8" FEP reactors heat-sealed at one end and capped with a stainless steel Swagelok fitting and Kel-F stem-tipped needle valve. Following the experimental descriptions of Biagioni[120], each reactor with its contents was attached to a metal vacuum manifold where a similar reactor containing liquid $S_2O_6F_2$ was also attached. The reactor

containing the carbon was evacuated. Under static vacuum and at room temperature the carbons were exposed to vapor $S_2O_6F_2$ in aliquots no greater than the room temperature vapor pressure of the liquid or approximately 130 torr. The pressure of the reactive gas was replenished every 30 minutes until no more uptake was observed by tensimetry. The total reaction time ranged from 1-4 hours. If a halogen flashlight was shined through the solid product, a blue hue was observed for all products. All volatiles were evacuated from the reactor and the solid was moved to an argon-purged glove box for storage and repackaging for analysis.

Conductivity measurements

During the synthesis of carbons by pyrolytic deposition, some material was deposited on a $1in^2$ quartz wafer placed in the middle of the reaction zone. The quartz wafer acquired a carbon film during the reaction and was handled under dry nitrogen after the reaction was complete. The conductivity of the film was measured using a Keithly 4-point probe fitted with a gold-contact 1cm bench installed in a nitrogen purged glove bag. The conductivity of the film was measured by direct contact. For comparison, anhydrous acetonitrile was used to rinse the films in an attempt to remove contaminants that may affect conductivity. The rinsed film was then dried by placing on a 100°C hot plate for 1 hour then the wafer was allowed to cool before measuring again. In all cases, the conductivity decreases somewhat after rinsing indicating either disruption of conductivity by the solvent directly or by removal of doping contaminants that enhance conductivity.

Purification of Pyrolytic Carbons

The pyrolytic C_5N and its pyrolytic carbon analog each were obtained as mixtures of lamellar and spherical structures; the lamellar structures being the desired ones. In addition

both could potentially have lower molecular weight impurities co-deposited in the matrix. Analysis of the carbons also indicated contamination by chlorine. Attempts to purify the products are described here.

Flotation methods were attempted in order to separate the lamellar carbon products from the spherical kind. This was done by placing a sample of the carbon in a glass vial and adding about 1 mL of dichloromethane in which all of the carbon rested on the bottom. Bromoform was added drop-wise to the liquid and allowed to equilibrate for 1 minute between each drop. Bromoform was added until some of the carbon began to rise from the bottom of the vial. The vial was allowed to equilibrate for one hour and samples were taken from the top and bottom for SEM analysis. All analyses indicated no difference in composition or morphology from the different samples.

Both carbon products were also treated with solvents in a Soxhlet extractor in an attempt to purify these of small molecules. NMP, DMF, and DMSO were passed through 1 gram of each carbon held in a quartz thimble for 24 hours. Each resulting solvent was evaporated away in an attempt to observe residue; no solid residues were obtained for any of the products indicating that any removable impurities were probably volatilized to cooler parts of the reactor during the synthesis.

Since chlorine contamination would apparently induce increased disorder and complexity to C_5N, its removal was attempted by a thermal annealing method. This was evaluated using a TGA-IR. Initially the sample was heated at 1°C per minute under a nitrogen purge of 90 sccm to see where chlorine loss would be prominent. It became apparent that at about 760°C chlorine content is lost in the form of ClCN which occurred simultaneously with additional cyanogens and traces of HCl (probably from the combination of ClCN and HCN). In an

attempt to give chlorine a donor atom to react with, pure H_2 gas was used in place of nitrogen. In this case, HCl was observed leaving at a temperature of 500°C but was accompanied by enormous quantities of HCN. Both of these experiments indicate the ability to remove chlorine contamination but compromising the nitrogen content. This apparent reductive instability may indicate why higher loadings of nitrogen could not be obtained for pyrolytic carbons by researchers who employed catalytic deposition methods where hydrogen is the expected byproduct.[121]

Another approach to chlorine removal was also attempted as described here. Since XPS analysis indicates that the chlorine contamination is primarily covalently bonded to sp^2 carbon, aggressive means of extraction seemed to be in order. Since the solid carbons are not soluble in any known solvent, they were suspended in a supporting medium. Heptane was chosen for its large liquid temperature range, somewhat suppressed flash point, its resistance to strong reducing agents, and its ability to wash away oils protecting certain reagents. For separate cases n-butyllithium in hexanes, methyllithium in pentane, lithium deuteride covered in mineral oil, and cyclohexyl magnesium chloride in ethyl ether were each used at -78°C and at room temperature. The reactions were quenched with D_2O give rise to deuterium substitution in the event of successful metallation.

The experimental procedure included placing 100mg of the carbon in a 25mL round bottom flask with 5ml of heptanes under an argon purge. After adjusting the reactor to the appropriate temperature, 1 mole equivalent of the reducing agent per six-membered unit of carbon atoms was added drop-wise with vigorous stirring from a glass-coated magnetic stir bar. After allowing the reduction to take place for 30 minutes, it was quenched by adding 1mL of D_2O. If necessary, the reactor was allowed to warm to room temperature, then 5 ml of water

was added and the resulting slurry was filtered through a 0.45 micron element and rinsed thoroughly with water to remove any inorganic salts.

The results were tracked by CHN and Cl elemental analysis[122]. In all cases and at both temperatures nitrogen content relative to carbon was significantly reduced (see results section). It is notable that elemental analysis also indicated almost quantitative removal of chlorine content in all experiments except those employing the cyclohexylmagnesium chloride where no reduction in chlorine content was observed. Following these attempts it was concluded that the best way to remove chlorine was to employ syntheses minimizing its incorporation by either optimizing yields or using reactants that do not contain halogens.

It was thus concluded for purposes of expediency that the synthesis procedure be optimized to make the most efficient use of chlorine by maximizing yields through allowing the longest possible kinetic soak time for the reactants in the reactor hot zone. This did not remove all chlorine, but significantly reduced its presence as apparent by XPS-ESCA and CHN & Cl analyses. This was chosen in contrast to methods described earlier utilizing alternative precursors devoid of chlorine as they gave poor stoichiometric yields on both an actual and theoretical basis.

Future Work

The structural characterization of poorly ordered materials remains a difficult task. In order to provide insight into the structures of truly graphitic carbon nitrides with sufficient nitrogen content such as C_5N, it will be necessary to eventually develop a synthetic method that will allow such a material to be studied. One method would be to develop a catalytic deposition method that does not produce a reducing byproduct such as hydrogen, possibly by using a

precursor such as cyanogen or tetracyanomethane. Another very promising idea provided directly by Dr. Landskron is to graphitize the pyrolytic C_5N as produced in this study under very high pressures and temperatures. Performed in a multi-anvil press, the high pressures used would, in theory, prevent nitrogen from escaping under the temperatures used in the annealing process. Even miniscule yields of the highly ordered C_5N products would prove invaluable to furthering the understanding of its chemical and structural nature, with the obvious application of re-attempting a demonstration of intercalation and allowing a more direct comparison with truly crystalline graphite rather than another poorly characterized analog.

Even without obtaining highly ordered C_5N materials, one may still wish to evaluate potential properties in alternative commercial applications. As a relatively broadly featured carbon, the current C_5N material may prove useful as an alternative to activated carbons for specialty purposes. Aside from the obvious future investigation of its surface adsorption properties related to inert gases, it may be desirable to exploit the potentially basic nature of the incorporated nitrogen atoms for acid trapping applications. Building on the observation that the current C_5N material appears to be reductively unstable, it may also prove an interesting material for the selective reaction and removal of undesirable contaminants in feed stocks such as hydrogen sulfide. Another possibly useful quality of this product is its conductivity coupled with its somewhat restricted oxidation onset potential relative to graphite itself. These electrical properties may prove useful in the growing field of fail-safe circuitry being deployed in ever-increasing numbers in modern electronics to make them safer to use and transport.

Another consideration of the current C_5N material is to use the nitrogen as a tether to chemically modify the surface in order to obtain properties not otherwise possible for pure carbons. Examples of such modifications could include N-oxides, hard-carbon based

quarternary amines, and solid-state azides. Each of these potential products could have possible applications in water purification, drug delivery, selective ion recovery, and in high-stability explosives.

Failing any of these endeavors, one has the option of waiting yet another 20 years for analytical advancements to enable absolute and finite characterization of the pyrolytic products obtained here. One plan in this area for the near future is to attempt the Neutron Diffraction elucidation of the complex structure in the C_5N material obtained in this study[123].

In all, any additional advances in the understanding of truly graphitic carbons with a sufficiently high nitrogen content to affect the bulk electronic environment and chemical properties will enable future scientists to realize their potential utility.

Conclusions

This work has been an attempt to evaluate an electron-rich graphite, one that is substantially substituted with nitrogen. The material selected from the literature is the only one reported to be graphite-like in nature and have considerable nitrogen content with an empirical formula of C_5N. Here the reproduction of the graphite-like synthesis was pursued and the product analyzed by a greater range of more advanced techniques. Its comparison with graphite was facilitated by the study of a pyrolytic carbon that was produced in exactly the same manner as C_5N. Finally, the attempted oxidative intercalation of all three materials was performed in order to complete the comparison.

The synthesis of C_5N by the pyrolytic condensation of chlorine with pyridine was reproduced with some difficulty as the original literature did not provide adequate experimental details. As a result the synthetic method was re-developed by scoping the major variables of

temperature, carrier gas, relative stoichiometry, absolute concentration, and alternative precursors. Because nitrogen loss is observed for C_xN materials at high temperatures, a helium carrier gas was employed with a reactor temperature of 700°C. The optimum chlorine to pyridine ratio was chosen at 5/2 as a balance between efficient use of chlorine and optimum yield. In an attempt to increase net yields, a powerful kinetic factor was discovered and yield was dramatically increased to nearly 75% isolated material relative to theoretical simply by increasing reaction residence time. Optimizing yield also reduced the contamination of the sample by chlorine and excess hydrogen. All of this is consistent with previous publications with the exception that yields were never reported by the originating authors.

The structural nature of C_5N as determined by numerous analytical methods was also generally consistent with earlier literature reports. The material is electrically conductive, bears extended sp^2 carbon centers with a mix of sp^2 and sp^3 nitrogens in addition to traces of hydrogen and chlorine contamination. Vibrational and micro-analytical methods indicate the material to be highly amorphous although some layering effects can be observed. Combined, these features confirm the current state of C_5N as graphite-like. While it may be tempting to assign the lack of order to the presence of the nitrogen and the potential for its random distribution throughout the matrix, the comparison of C_5N with its analog produced from the reaction of benzene with chlorine indicated that the synthetic method is the most likely origin of poor order. The amorphous solids obtained from both were composed of morphologies represented by both lamellar and spherical particles, the latter of which was not reported in the original literature. The redox properties of the carbons produced in this study directly confirm the lower oxidation onset potential of the nitrogen containing substrate as was expected.

Consistent with many other solid state synthesis examples, the numerous attempts to anneal or purify C_5N were unsuccessful. In the process of these attempts, it was discovered that the nitrogen content of C_5N was easily compromised in the presence of reducing agents such as hydrogen and alkyl organometallics at temperatures where the compound is otherwise stable. Although this latter point has not been discussed in the literature, it appears that it may represent one of the reasons why researchers world-wide have routinely produced nitrogen-poor examples of C_xN resulting from the presence of reducing catalysts in addition to the expected generation of other reducing byproducts such as ammonia and hydrogen gases.

The reaction of $S_2O_6F_2$ with C_5N, its benzene analog, and graphite was also performed in this study. While this interaction is known for graphite, it has never been reported for the other two pyrolytic materials. All three compounds adopted a blue color upon reaction with the peroxide indicating at least some degree of true inter-layer intercalation. The uptake of peroxide decreased from graphite>>C_5N>Benzene analog. Careful analysis of all three materials indicated a bonding of the fluorosulfate adduct to carbon. This was unexpected for C_5N where the oxidation was expected at the nitrogen atom and may be an indication that the nitrogen is simply behaving as an activating specie rather than a reactant site. Empirical and first principle evidence of actual intercalation of graphitic domains was only seen for the graphite and the benzene analog cases. We found no direct evidence of any extended layering of C_5N. It was noted that order of all three samples was severely compromised upon treatment with $S_2O_6F_2$.

This work has confirmed and thereby reactivated previous knowledge about C_5N. However, it has been discovered in the process that it is not as highly ordered as the original founding literature might have led one to believe. Future studies in this area would most likely be centered on attempts to improve order rather than yield either by improved synthetic

methodologies or by treatment methods of the currently available C_5N to induce order. In addition, the advent more powerful analytical methods in the future may help glean even more information from the current system which has now been described in sufficient detail for direct and nearly exact reproduction.

References

[1] J. Kouvetakis, R. Kaner, M. Sattler, and N. Bartlett. *J. Chem. Soc., Chem. Comm.* (1986) 1758-9.
[2] J. Kouvetakis, N. Bartlett, et al. *Synth. Metals.* 34 (1989) 1-7.
[3] C. Shen. *Ph.D Dissertation.* University of California, Berkely. (1992).
[4] D. Williams. *J. Chem. Soc.* (1931) 2783-7.
[5] P. Trowbridge and O. Diehl. *J. Am. Chem. Soc* 19 (1897) 558-74.
[6] C. Shen, N. Bartlett, et al. *J. Solid State: Chem.* 147 (1999) 74-81.
[7] J. Kouvetakis, N. Bartlett, et al. *Synth. Metals.* 34 (1989) 1-7.
[8] M. Labes. US Patent 5143709. 1992.
[9] Labes. World Pat. App. 90/15776. 1990.
[10] D. Kim and M. Labes. *Chem. Mater.* 2 (1990) 599-603.
[11] D. Kim and M. Labes. *Mat. Res. Bull.* 25 (1990) 1461-5.
[12] D. Kim, C. Lin, T. Mihalisin, P. Heiney, and M. Labes. *Chem. Mater.* 3 (1991) 686-692.
[13] P.-H. Chang and M. Labes. *Chem. Mat.* 1 (1989) 523-5.
[14] V. Skarda, D. Ivkovich, and M. Labes. *J. Poly. Sci. Poly. Chem. Ed.* 23 (1985) 107-17.
[15] J. Chen and M. Labes. *Macromol.* 19 (1986) 1528-30.
[16] J. Chen and M. Labes. *Macromol.* 18 (1985) 827-8.
[17] J. Chen and M. Labes. *J. Poly. Sci. Poly. Chem. Ed.* 23 (1985) 517-23.
[18] V. Ageev, M. Ugarov, E. Loubnin, and V. Konov. *SPIE.* 3484 (1998) 25-32.
[19] T. Nakajima, M. Koh, and T. Katsube. *Solid State Sci.* 2 (2000) 17-29.
[20] M Terrones, W. Hsu, H. Kroto, and D. Walton. *Topics Current Chem.* 199 (1999) 189-234.
[21] A. Liu and M. Cohen. *Science.* 245 (1989) 841-2.
[22] T. Malkow. *Mat. Sci. Eng.* A292 (2000) 112-124.
[23] T. Malkow. *Mat. Sci. Eng.* A302 (2001) 311-324.
[24] D. Miller, J. Wang, and E. Gillan. *J. Mater. Chem.* 12 (2002) 2463-9.
[25] J. Wang, E. Gillan. *Thin Solid Films.* 422 (2002) 62-68.
[26] E. Gillan. *Chem. Mater.* 12 (2000) 3906-3912.
[27] D. Walton, et al. *Adv. Mater.* 11, 8 (1999) 655-658.
[28] M. Koh, T. Nakajima, R. Singh. *Mol. Cryst. Liq. Cryst.* 310, 1 (1998) 341-6.
[29] J. Wang, D. Miller, and E. Gillan. *Carbon.* 41 (2003) 2031-7.
[30] T. Nakajima, M. Koh, and T. Katsube. *Solid State Sci.* 2 (2000) 17-29.
[31] I. Shimoyama, G. Wu, T Sekiguchi, and Y. Baba. *J. Elect. Spect. Related. Phenom.* 114-116 (2001) 841-8
[32] I. Shimoyama, G. Wu, T. Sekiguchi, and Y. Baba. *Phys. Rev. B.* 62, 10 (2000) R6053.
[33] H. Chen, Y. Yang, Z. Hu, K. Huo, Y. Ma, Y. Chen, X. Wang, and Y. Lu. *J. Phys. Chem. B.* 110, 33 (2006) 16422-7.
[34] G. Barucca, G. Majni, P. Mengucci, et al. *J. App. Phys.* 86, 4 (1999) 2014-9.
[35] T. Sekine, H. Kanda, Y. Bando, M. Yokoyama, and K. Hojou. *J. Mat. Sci. Lett.* 9, 12 (1990) 1376-8

[36] A. Liu and M. Cohen. *Phys. Rev. B.* 41, 15 (1990) 10727.
[37] A. Ferrari, S. Rodil, and J. Robertson. *Phys. Rev. B.* 67 (2003) 155306/1-6.
[38] W. Sucasaire, M. Matsuoka, K. Lopes, J. et al. *J. Braz. Chem. Soc.* 17, 6 (2006) 1163-9.
[39] E. D'Anna, M. De Giorgi, A. Luches, M Martino, A Perrone, and A Zocco. *Thin Solid Films.* 347 (1999) 72-7.
[40] I. Gouzman, R. Berner, and A. Hoffman. *J. Vac. Sci. Tech. A.* 17, 2 (1999) 411-20.
[41] Q. Guo, Q. Yang, C. Yi, L. Zhu, and Y. Xie. *Carbon.* 43 (2005) 1386-91.
[42] D. Miller, J. Wang, and E. Gillan. *J. Mat. Chem.* 12 (2002) 2463-9.
[43] H. Chen, Y. Yang, Z. Hu, K. Huo, Y. Ma, and Y. Chen. *J. Phys. Chem. B.* 110 (2006) 16422-7.
[44] M. dos Santos and F. Alvarez. *Phys. Rev. B.* 58, 20 (13918-24).
[45] T. Sekine, H. Kanda, Y. Bando, M. Yokoyama, and K. Hojou. *J. Mat. Sci. Lett.* 9 (1990) 1376-8.
[46] Y. Ma, A. Foster, A. Krasheninnikov, and R. Nieminen. *Phys. Rev. B.* 72, 20 (2005) 205416/1-6.
[47] B. Zheng. W. Zheng, K. Zhang, Q. Wen, J. Zhu, S. Meng, X. He, and J. Han. *Carbon.* 44 (2006) 962-8.
[48] A. Snis and S. Matar. *Phys. Rev. B.* 60, 15 (1999) 10855.
[49] J. Yasinsky and S. Ergun. *Carbon.* 2 (1965) 355-8.
[50] F. Tuinstra and J. Koenig. *J. Chem. Phys.* 53, 3 (1970) 1126-30.
[51] C. Brundle, et al, eds. *Encyclopedia of materials characterization.* Butterworth-Heinemann, Boston, 1992.
[52] H. Kuzmany. *Solid state spectroscopy.* Springer, New York, 1998.
[53] W. Rudorff. *Adv. in inorg. Chem. and radiochem.: V1.* H. Emeleus ed., Academic Press, New York, 1959. 223-66.
[54] T. Enoki, et al. *Graphite intercalation compounds and applications.* Oxford University Press, New York, 2003.
[55] Y.-O. Kim and S.-M. Park. *J. Electrochem. Soc.* 148, 3 (2001) A194-9.
[56] H. He, T. Riedl, A. Lerf, and J. Klinowski. *J. Phys. Chem. B.* 100 (1996) 19954-8.
[57] J. Giraudet, M. Dubois, A. Hamwi, W. Stone, P. Pirotte, and F. Masin. *J. Phys. Chem.* 109 (2005) 175-81.
[58] H. Wang and M. Yoshio. *Electrochem. Comm.* 8 (2006) 1481-6.
[59] T. Nakajima, M. Koh, and M. Takashima. *Electrochem. Acta.* 43, 8 (1998) 883-91.
[60] D. Zhong, G. Zhang, S. Liu, E. Wang, Q. Wang, H. Li, and X. Huang. *App. Phys. Lett.* 79, 21 (2001) 3500-2.
[61] T. Nakajima and M. Koh. *Denki Kagaku oyobi Kogyo Butsuri Kagaku.* 64, 8 (1996) 917-8.
[62] M. Koh, T. Nakajima, and T. Singh. *Mol. Cryst. Liq. Cryst.* 310, 1 (1998) 341-6.
[63] M. Koh, H. Yumoto, H. Higashi, and T. Nakajima. *F. Fluor. Chem.* 97 (1999) 239-46.
[64] T. Nakajima and M. Koh. *Carbon.* 35, 2 (1997) 203-8.
[65] T. Nakajima, M. Koh, and T. Katsube. *Solid State Sci.* 2 (2000) 17-29.
[66] J. Xia and F. Aubke. *J. Fluor. Chem.* 57 (1992) 53-63.
[67] T. Nakajima, ed. *Fluorine-carbon and fluorine-carbon materials.* Marcel Dekker, Inc., New York, 1995.
[68] R. Hagiwara, M. Lerner, and N. Bartlett. *J. Chem. Soc. Chem. Comm.* (1989) 573-4.
[69] J. Hoogley. *Carbon.* 21, 3 (1983) 181-8.
[70] S. Karunanithy and F. Aubke. *Mat. Sci. Eng.* 62 (1984) 241-8.
[71] S. Karunanithy and F. Aubke. *J. Chimie Physique.* 81 (1984) 827-33.
[72] S. Karunanithy and F. Aubke. *Carbon.* 20, 3 (1982) 237-41.
[73] N. Bartlett, R. Biagioni, B. McQuillan, A. Robertson, and A. Thompson. *J. Chem.Soc. Chem. Comm.* (1978) 200.
[74] M. Wechsberg, P. Bulliner, F. Sladky, R. Mews, and N. Bartlett. *Inorg. Chem.* 11, 12 (1972) 3063-70.
[75] F. Dudley and G. Cady. *J. Am. Chem. Soc.* (1957) 513-4.
[76] N. Bartlett, M. Wechsberg, F. Sladky, and P. Bulliner. *J. Chem. Soc. Chem. Comm.* 703-4.
[77] D. Zhang, C. Wang, F. Mistry, B. Powell, and F. Aubke. *J. Fluor. Chem.* 76 (1996) 83-9.
[78] F. Dudley. *J. Chem. Soc.* (1963) 3407-11.
[79] J. Coleman and D. Pletcher. *Tet. Lett.* (1974) 147-50.

[80] F. Dudley and G. Cady. *J. Am. Chem. Soc.* (1963) 3375-7.
[81] J. Shreeve and G. Cady. *J. Am. Chem. Soc.* (1961) 4521-5.
[82] A. West. *Solid state chemistry and its applications.* John Wiley & Sons Ltd., New York, 1984.
[83] A. Cheetham and P. Day, eds. *Solid state chemistry techniques.* Oxford University Press, New York, 1987.
[84] B.L. Weiss, et al. *Properties of Amorphous Carbon.* INSPEC, London, 2003.
[85] J. Wang, D. Miller, and E. Gillan. *Carbon.* 41 (2003) 2031-7.
[86] K. Nakamoto. *Infrared and Raman Spectra of Inorganic and Coordination Compounds.* Wiley, New York, 2008.
[87] J. Williamson, et al. *Fuel.* 78 (1999) 803-7.
[88] E. Trasobores, et al. *J. Elect. Spect.* 56 (2002) 1721-34.
[89] D. R. Lide, et al. eds. *CRC Handbook of Chemistry and Physics: 75th Ed.* CRC Press, Ann Arbor, MI, 1994. Section 12 Pp. 43
[90] P. Rieger. *Electron Spin Resonance: Analysis and Interpretation.* Springer, New York, 2007. Pp 223.
[91] F. Rivadulla, et al. *Phys. Rev. B.* 60, 17 (1999) 11922-5.
[92] P.T. Kissinger, et al. eds. *Laboratory Techniques in Electroanalytical Chemistry.* Marcel Dekker, New York, 2006. Pp. 223.
[93] N. Bartlett, et al. *Inorg. Chem.* 11, 12 (1972) 3063-70.
[94] R. Biagioni. Ph.D. Thesis: "Fluorosulfates of Graphite and Boron Nitride". U. of California, Berkeley. 1981.
[95] Ace Glass part # 7531-10 – Glass bubbler/impinger
[96] Carbolite part # MTF 10/15/130
[97] R. Mann and M. Van der Meulen. *J. Chem. Soc.* 53 (1931) 451-3.
[98] J. Dean, ed. *Lange's Handbook of Chemistry:. 12th Edition.* McGraw-Hill, New York, 1979.
[99] Omega Corporation. *The Flow and Level Handbook.* Omega Engineering, Inc., Stamford, CT, 2000.
[100] Aldrich product # 271004
[101] Meinhard, Type A3 Nebulizer, part # WE024371
[102] Alfa Aesar, platinum gauze – 100 mesh – part # 10282
[103] Bioanalytical Systems part # MW-1033
[104] Bioanalytical Systems, cell vial, part # MF-1082
[105] Bioanalytical Systems, vial top/electrode holder, part # ER-8946
[106] T. Nakajima, et al. *Electrochimica Acta.* 3, 8 (1998) 883-91.
[107] Aldrich product # 450227
[108] Aldrich product # 676802
[109] Aldrich product # 517127
[110] N. Bartlett, et al. *Inorg. Chem.* 11, 12 (1972) 3063-70.
[111] FEP is a register trademark of the DuPont Corporation
[112] Zeus Industrial Products – I/2 in O.D. Heavy wall standard tubing
[113] Swagelok part # SS-810-R-4
[114] Swagelok part # PFA-43S4
[115] Swagelok part # SS-400-3-2-4-BT
[116] Swagelok part # SS-1KS4
[117] Aldrich, XeF_2, part # 394505
[118] Aldrich FSO_3H, Triple-distilled, part # 236535
[119] G. Cady and F.Dudley. *J. Am. Chem. Soc.* 79 (1957) 513-4.
[120] R. Biagioni. Ph.D. Thesis: "Fluorosulfates of Graphite and Boron Nitride". U. of California, Berkeley. 1981.
[121] T. Nakajima and M. Koh. *Carbon.* 35, 2 (1997) 203-8.
[122] CHN and Cl analysis were performed by Schwarzkopf Laboratories, NY.

[123] C. Brown and J.-H. Her at NIST, Gaithersburgh, MD.

Appendix A: Researcher's Biography

Wade H. Bailey III was born on March 3, 1976 at Kirtland Air Force Base, NM. His parents Wade (Jr.) and Cathy Bailey were career Air Force officer and dedicated secondary school teacher, respectively. After graduating from Lewis Palmer High School of Monument, CO in 1993, Wade matriculated in chemistry for two years at Philips University in Enid, OK. After a working foray, a Bachelors of Science in Chemistry was obtained with the honors of *Magnum-cum-Laude* at Colorado State University at Pueblo, CO in 1998.

Wade moved with his wife, Julie, and step daughter, Monique, to Allentown PA where he began his working career as a research chemist at Air Products and Chemicals, Inc., training in the art of fluorine and reactive gas chemistry. Experience and training were expanded over the next ten years into areas of selective fluorination, fluorinating agents, pharmaceutical intermediates, advanced analytical applications systems, optical liquid crystals, novel functional groups, electrochemical methods, and lithium-ion battery electrolytes. In 2000, matriculation with Lehigh University, Bethlehem, PA was commenced ending (2008) with the culmination of the work presented here as a collaborative thesis between Air Products and the University.

Below is list of selected publications authored or co-authored by this researcher:

W. Casteel, et al. US Patent 6307105. "High Purity Preparation of Fluorinated 1,3-Dicarbonayls Using BDM". 2001.

W. Casteel and W. Bailey. US Patent 6455728. "Direct Fluorination Process for Preparing High Purity 2-Fluoro-1,3-dicarbonyl compounds using oxygen as a radical scavenger". 2002.

R. Syvret, et al. *Collect. Czech. Chem. Commun.* 67 (2002) 1416-20.

W. Bailey and W. Casteel. US Patent 6869582. "Process for the Synthesis of $BrSF_5$". 2005.

W. Bailey, et al. US Patent 7015176. "Process for the Synthesis of Aryl Sulfurpentafluorides". 2006.

W. Bailey, et al. US Patent 7025901. "Alkyl and Aryl Trifluoromethoxytetrafluorosulfuranes". 2007

W. Bailey, et al. US Patent 749671. "Process for the Fluorination of Boron Hydrides". 2008.

END OF TITLE